2008

Development and Characterization of a Mechanically Prestressed Piezoelectric Composite

Byron Fitzgerald Smith
Virginia Commonwealth University

DEVELOPMENT AND CHARACTERIZATION OF A MECHANICALLY PRESTRESSED PIEZOELECTRIC COMPOSITE

A thesis submitted in partial fulfillment of the requirements for the degree of Master of Science at Virginia Commonwealth University.

by

BYRON F. SMITH
Mechanical Engineering, Virginia Commonwealth University

Director: DR. KARLA MOSSI
ASSOCIATE PROFESSOR, MECHANICAL ENGINEERING

Virginia Commonwealth University
Richmond, Virginia
May, 2008

Acknowledgement

The progression of this work has been, if nothing else, a humbling experience. While I have learned many things in the course of my studies, I feel that the most important knowledge that has been imparted on me is the value of inspiration. With that said, I would like to thank those individuals who have been most inspiring to me during this journey.

First and foremost, I'd like to thank my advisor, Dr. Karla Mossi. Your guidance, wisdom, and example have been instrumental in developing my character both as a researcher and as an individual.

I owe a special thanks to Dr. Zoubeida Ounaies for showing me that there is more to school than receiving high marks. For sharing your passion and enthusiasm, I will be forever grateful.

I would like to thank Dr. Robert Bryant for sharing his intellectual insights with me, but more so, I'd like to thank him for sharing that which can never be written down for fear they might identify the author.

Of course, if it were not for my family and friends none of this ever would have been possible. I believe that we are what those we care about us most expect us to be, and I am thankful that those closest to me have each expected so much of me. In particular, I'd like to think Terry Hegwood, Kyle Paul, Rachel Smith, Nicolas Castro, Poorna Mane, Roy Ludi, Kelly Huang, Matt Kazmier, and Joel Driskell for all their inspiration and support.

I would like to thank Teresa Bobbio and Dan Smith for their unwavering support and belief.

And last but not least, I'd like to thank my committee member, Dr. Kam Leang, for providing inspiration and rigor.

Table of Contents

Page

List of Tables

Page

List of Figures

Page

Nomenclature

ε ……....Strain $\left(m/m\right)$

R_n …….....Radius of the Neutral Axis $\left(m\right)$

σ ……...Stress $\left(N/m^2\right)$

E ……...Young's Modulus $\left(N/m^2\right)$

ν ……....Poisson's Ratio

M …….....Moment $\left(N \cdot m\right)$

I ……....Second Moment of Area $\left(m^4\right)$

σ_u ……..Ultimate Tensile Stress $\left(N/m^2\right)$

k ……Spring Constant $\left(N/m\right)$

D ……...Center Displacement Constant $\left(kV/m^2\right)$

Abstract

DEVELOPMENT AND CHARACTERIZATION OF A MECHANICALLY PRESTRESSED PIEZOELECTRIC COMPOSITE

By Byron F. Smith, B.S.

A thesis submitted in partial fulfillment of the requirements for the degree of Masters of Science at Virginia Commonwealth University.

Virginia Commonwealth University, 2008

Major Director: Karla Mossi, Ph.D.,
Associate Professor, Mechanical Engineering

Piezoelectric composites have been investigated for use in a variety of areas, including flow control, structural control, energy harvesting, and fuel ignition systems. While many of the investigations conducted in these areas have utilized traditional piezo actuation systems, such as unimorphs or stack actuators, a growing number of research groups are examining the increased performance derived from the mechanical advantage, and enhanced domain rotation, found in prestressed unimorph designs. Prestressed devices, like Thunder® and LIPCA, have been shown well suited for a number of applications; however, the price associated with these devices can often prevent them from being

implemented. In an effort to produce a low cost unimorph device that possesses a performance-enhancing curved form, the present investigation presents a novel technique for manufacturing prestressed piezoelectric actuators that are capable of meeting the same high displacement and load bearing capabilities exhibited by conventional prestressed devices.

The newly proposed mechanically prestressed composite device, or MPC, is similar in form and function to well-documented thermally prestressed devices like Thunder®. However, rather than deriving its characteristic curved form from a thermally induced stress, the present class of devices relies on the resorting force incited in the piezoelectric ceramic upon adhesion to a mechanically deformed substrate to provide both the performance-enhancing prestress and final form of the device. To aid in refinement of the newly proposed design, beam theory was used to model the stress developed within the device. The model allowed designers to investigate the limitations imposed on the performance-enhancing curved form of the device by the stresses developed in the ceramic as a result of the curvature. Findings derived from the model were experimentally verified before a finalized design was specified for the composite, and a number of devices were manufactured.

An initial characterization of the device was carried out based on the composite's response to mechanical and electrical loading. By determining the slope of the electrically and mechanically induced displacement response of the device, the investigation was able to define the center displacement constant and effective spring constant of the unimorph. These parameters not only allow designers to predict the displacement that will occur in

response to a given electric field or tensile load, but also to allow for comparison with various devices. In the present investigation, the performance characteristics of mechanically prestressed composites were assessed as a function of substrate thicknesses and adhesive properties. With composites constructed using substrates approximately 9.2cm in length, devices were found to have typical center displacement constants on the order of 1.59 to 7.78 kV/mm^2 while retaining an effective stiffness between 4.5 to 7.5 N/mm. These values were found to be similar to the .71 to 3.85 kV/mm^2 center displacement constants demonstrated by similarly sized and shaped Thunder® devices, which posses an effective stiffness in the range of 10 to 16.3 N/mm. A comprehensive presentation of the test methods and procedures used to determine these values, along with other performance characteristics, are provided.

CHAPTER 1

1. Introduction

This thesis presents both a novel method for constructing piezo-composite unimorph devices and a characterization of several devices constructed using the newly proposed technique. The objective of this work is to develop, manufacture, and characterize a high performance unimorph device, based on a novel design allowing for the reduction of manufacturing costs. Currently, two distinctive unimorph architectures are commercially available. These two architectures consist of a traditional, flat laminate form, and a thermally prestressed, curved form. Devices constructed utilizing the traditional design consist of a piezoelectric plate adhered to an elastic substrate. While these devices are inexpensive and easy to construct, they are unable to achieve the enhanced performance characteristics that an emerging class of curved-prestressed unimorphs are capable of displaying. Curved-presstressed devices are able to support greater loads than their flat counter parts, while achieving comparable displacement, all without sustaining mechanical damage. They are able to achieve such feats due to the mechanical advantage provided by their curved form: this advantage, however, is gained at appreciable cost. To illustrate the magnitude of these tradeoffs, consider that a traditional unimorph bender can be purchased for approximately one tenth the cost of a comparable prestressed device. The

prestressed devices, however, are capable of producing approximately forty percent more displacement [2-4]. This example demonstrates the marked increase in performance that can be achieved from utilization of a prestressed form as well as the significant increase in cost associated with thermal processing of these devices. While a number of prestressing methods have been documented in the literature, thermally processed devices, with their performance enhancing curved from, are one of the few prestressing methodologies that have achieved sustained commercialization [5-7]. Since a high percentage of the cost associated with these prestressed unimorphs can be attributed to the manufacturing processes, new methods of applying prestress need to be developed in order to reduce device costs. Therefore, the need to reduce manufacturing related expenses motivates the effort to develop a novel prestressed unimorph design.

Specifically, this thesis evaluates the performance achieved by a newly presented prestressed composite design. The mechanically prestressed composite design, or MPC, is capable of producing a device that displays performance characteristics comparable to those demonstrated by thermal prestressed unimorphs. MPC devices have the benefit of mitigating many of the costs associated with thermally prestressed unimorph devices since the manufacturing of these devices does not require thermal processing techniques. Figure 1.1 provides a comparison of the manufacturing processes used in the construction of thermally prestressed actuators, such as Thunder®, and the newly proposed mechanically prestressed devices.

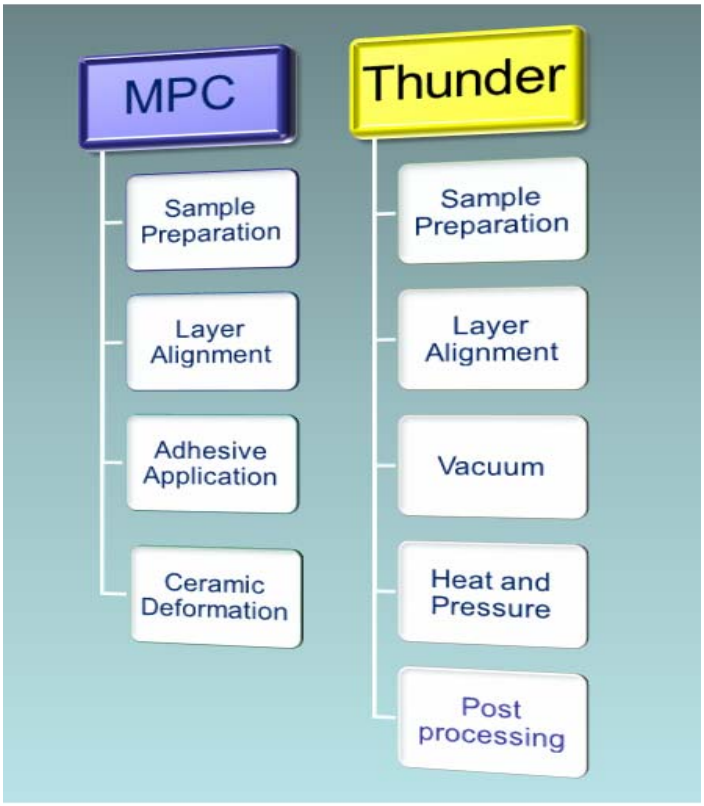

Figure 1.1 Flowchart of MPC and Thunder® manufacturing processes.

To determine the relative merit of the new class of devices, performance characteristics deemed significant by previous investigations were experimentally determined and compared with the characteristics of other devices documented in the literature. Several design variables were investigated, and the magnitude to which these variables affect device performance was assessed. While it should be noted that the new device was found to perform comparably to existing prestressed devices, the results indicate that further design analysis will allow for optimization and increased performance.

The work presented in this thesis is significant because the results presented can be used to help researchers design and construct inexpensive, high performance unimorph

devices. With unimorph devices currently being investigated for use in applications such as flow control, energy harvesting, and structural health monitoring, optimum design is of utmost importance in the development of applications.

1.1 Thesis Goal

The main goal of this work focuses on creating a prestressed piezoelectric device that lends itself to low cost manufacturing while retaining the levels of performance currently demonstrated by commercially available devices. Noting that the performance of commercial devices is largely owed to the mechanical advantage gained by way of its prestressed from, the investigation utilizes beam theory to determine the theoretical limitation that stress imposes on the curvature of such a unimorph device. Experimental verification of the analytically derived design limitations allowed for refinement of the design prior to specifying a finalized configuration. The advantage of utilizing beam theory arrives from the simplicity with which it allows for determination of design limitations, while experimental verification of these limits allowed for the assessment of various construction methodologies.

To assess attainment of the goal, an initial evaluation of the performance characteristics of the newly proposed unimorph was undertaken. Previous investigations have set a precedence of assessing the performance of such devices based on total displacement and strains developed in response to a number of loading conditions. In order to provide a relative measure to findings, the performance characterization of the newly

proposed device is carried out using test equipment and procedures that have been utilized in the characterization of similar devices.

1.2 Outline

This thesis is organized as follows. Chapter 2 is an introduction to the field of smart materials and structures. It expands on the motivations behind the work presented in this thesis and introduces some of the more general motivations which drive developments throughout the field of smart materials. An overview of some common smart materials is provided, followed by an outline of the historical developments in piezoelectricity and the chronological progression of piezoelectric actuators. The chapter concludes with a brief summary of the challenges associated with unimorph design and the successful implementation of unimorph technology.

Chapter 3 presents the analytical development of the mechanically prestressed composite unimorph design. The analytical treatment begins by defining the governing equations of the device and then continues to show how these equations provide the theoretical limitations placed on the post-manufactured form of the unimorph. Results of the experimental verification of the design limitations are given and details concerning the finalized design configuration are specified.

Chapter 4 reveals the manufacturing processes and outlines steps taken to ensure the quality of the manufactured device. Chapter 5 provides details concerning equipment and procedures used during the course of the performance evaluation. Results of the evaluation are presented in Chapter 6. Finally, concluding remarks and suggested

directions for the course of future works are given in Chapters 7 and 8, respectively. Appendices documenting results not presented in the body of the work and subsidiary analysis can be found at the end of this document.

CHAPTER 2

Smart Materials and Structures

Smart materials have been defined in the literature as materials that possess the "unique capabilities to adapt to changes and external stimuli capitalizing on the intrinsic intelligence embedded in them" [8]. These materials are often used as an actuator, a sensor, or both. A growing area of interest in the field of smart materials is the incorporation of hybrid devices that function as both actuators and sensors in structures that are capable of detecting and responding to changes in their environment. These structures have come to be known as "smart structures" due to their ability to sense and respond to external stimuli. De Boer first presented the study of structures that incorporated the use of actuators and sensors to optimize a system's performance in 1961 [9]. Since De Boer's work, continued effort has been expended in the development of feedback-based vibration control techniques that utilize a variety of both traditional and smart materials. These efforts demonstrate the continued interest of research in the areas of materials development, structural dynamics, and structural controls.

While many of the characteristics of smart materials have been well documented in the literature for more than half a century, a great majority of the applications for which they have become well-known have only recently come to market. Examples of smart

materials and some of the applications in which they are currently being used can be seen in arterial stents made from shape memory alloys, magnetorestrictive sonar units, and piezoelectric positioning systems, to name a few [10]. Products such as these showcase the vast array of areas in which smart materials' research is applicable and the ingenious manners in which engineers are able to utilize the properties of these materials.

Many of the most commonly utilized smart materials can be actuated through the use of an electrical potential. The means by which that potential elicits a response, however, can vary from one material to the next. In the case of piezoelectric ceramics and polymers, the application of an electric field across a material will induce a strain. When actuating a Shape Memory Alloy, or SMA, an electric current must be used to generate resistive heating in order to produce a physical stimulus to which the material will respond. If a similar electric potential is to instigate a response from magnetorestrictive alloys, it must be used to generate an electromagnetic field. Given the different mechanisms by which various smart material are actuated it is easy to comprehend how certain smart materials are better suited for particular applications than others. In order to gain a better understanding of the relationship found between a given smart material and the stimuli which is used to elicit a response from that material, it is informative to examine the mechanics found presently in applications which motivate the use of the material.

2.1 Motivation

Many of the active and passive vibration control techniques that have been proposed in the literature utilize smart materials due to the high energy density levels these

materials possess [11]. Feasibility studies conducted at the Los Alamos National Laboratory, by Park et al., illustrate ingenious usages for passively dissipated vibrational energy in applications such as wireless structural health monitoring [12]. Investigations such as those conducted by Park et al., Granstrom et al., and Anderson et al., have sparked the interest of research groups around the world regarding the capabilities of smart materials in the areas of energy harvesting, vibration control, and structural health monitoring [12-14]. While some research groups develop novel actuators and transducers to facilitate their investigations in these areas, a great number of research groups are performing investigations that utilize off-the-shelf actuators and transducers.

The demand for consumer ready devices that are capable of servicing researchers' needs in the areas of vibration control, energy harvesting, and a number of other fields, has led to the development of numerous devices that are capable of providing both actuation and sensor based functions. Devices like unimorphs, bimorphs, stacks, Rainbow, Thunder®, and piezoelectric micro fiber composites are but a few of the many products that demonstrate the engineering community's efforts to meet the need for consumer ready devices in these areas of interest. The continuously growing body of work regarding hybrid smart devices is a testament to researchers' ongoing efforts in the development of more cost-effective and efficient devices. In the present investigation, these goals are sought by way of eliminating the need for thermally processing prestressed unimorphs. By mechanically prestressing the devices substrate prior to consideration of the composite, manufactures are able to achieve a prestressed device that has the same form and function as a thermally prestressed device without necessitating expensive autoclaves or exotic

adhesives like LaRC-SI. Eliminating thermal processing also helps to reduce manufacturing cost by eradicating the need to repole devices following the thermally induced relaxation of dipoles.

In order to provide the reader with a working knowledge of the general characteristics of various smart materials and devices utilizing these materials, which constitute the forefront of the field's present focus, a brief overview of commonly utilized smart material follows.

2.2 Common Smart Materials

While the materials presented in this section are some of the most commonly utilized smart materials, it would be a grave overstatement to assert that any of these materials are ubiquitous. It should also be noted however, that, while the below outline presents an eclectic array of smart materials and smart material-based technologies, it is by no means a complete index of the smart materials currently being investigated by researchers.

2.2.1 Magnetorestrictive Alloys

James Joule first discovered in 1842 that a ferromagnetic crystal changes its shape in the presence of a changing magnetic field. He termed this phenomenon the "magnetorestrictive effect." One of the most commonly used magnetorestrictive alloys was developed at the Naval Ordinance Laboratory and is referred to as Terfenol-D. Terfenol-D has an energy density greater than piezoelectric materials and is capable of

obtaining strains up to two tenths of a percent [10]. Other advantages that magnetorestrictive alloys enjoy over piezoelectric materials include reliability, stable material properties, and flexibility [10]. A disadvantage of these alloys, however, is the difficulties encountered during production, a difficulty attributed to impurities in the basic materials from which these alloys are derived. Other shortcomings include the high reactivity of the rare-earth materials that comprise magnetorestrictive alloys and the requirement of relatively large magnetic fields for actuation [10 , 15].

2.2.2 Shape Memory Alloys

Shape memory alloys, or SMA's, are materials that are capable of returning to their original form after being deformed upon the introduction of a thermal stimulus. This behavior is a result of the reversible transformation of the material's crystalline structure from the martensite phase to the austenite phase [16]. In the 1950s, William Buehler discovered the shape memory effect within certain copper alloys and, in subsequent years, the effect was also found in nickel titanium alloys [10]. While the thermally-induced deformations are highly hysteretic, one advantage of using SMA's as an actuator lies in the ability of designers to tailor the temperature at which structural transformation occurs within a range of –200 to +200^{o}C simply by altering the alloys' compositions [17]. One application that has effectively utilized SMA's is found in the S.M.A.R.T.® Stent [18].

S.M.A.R.T.® Stents, produced by the Cordis Corporation, were first introduced in 1999, and in 2003 they received FDA approval for the treatment of patients with symptomatic atherosclerotic disease [18, 19]. Atherosclerotic disease is the progressive

narrowing and hardening of the arteries due to plaque buildup. S.M.A.R.T.® Stents employ a particularly well-suited actuation method to open these clogged arteries by utilizing the shape memory effect of Nitinol. Nitinol is a biocompatible nickel-titanium alloy developed at the Naval Ordinance Laboratory. When a S.M.A.R.T.® Stent is inserted into a clogged artery, it uses the body's heat to stimulate the shape memory effect, returning the device to its un-deformed shape, which in turn allows blood to flow through the artery.

2.2.3 Electrorheological Fluids

At the end of the nineteenth century, it was known that a moderate electric field (0.1 to1 kV/mm) could increase the viscosity of certain liquids by up to one hundred percent. However, in the 1940s, Willis Winslow discovered that he was able to obtain much higher viscosity increases in what would soon be called "electrorheological fluids" [20]. The fluids that Winslow produced were suspensions of solid and non-metal hydrophilic particles with small amounts of absorbed water in non-conductive oils and solvents [21]. These fluids were found to solidify when exposed to an electric field, demonstrating the coupling between their fluid dynamic and electrical properties. This significant increase in viscosity, and the shear strength exhibited upon exposure to an electric field, made them ideally suited for many applications, ranging from shock absorbers to active structure control [22].

2.2.4 Piezoelectric Materials

Piezoelectricity is defined by Jaffe, Cook, and Jaffe as the "ability of certain crystalline materials to develop an electric charge proportional to a mechanical stress" in their classical work on the subject [15]. The discovery of this phenomenon is attributed to two brothers, Jacque and Pierre Curie. In 1880, these two men presented their work, *Development by pressure of polar electricity in hemihedral crystals with inclined faces,* which stated [23]:

> *Those crystals having one or more axes whose ends are unlike, that is to say hemihedral crystals with oblique faces, have the special physical property of giving rise to two electrical poles of opposite signs at the extremities of these axes when they are subjected to a change in temperature: this is the phenomenon known under the name of pyroelectricity…We have found a new method for the development of polar electricity in these same crystals, consisting in subjecting them to variations in pressure along their hemihedral axes.*
>
> P. & J. Curie

Not long after this discovery, a contemporary of the Curies' by the name of Wilhelm Hankel suggested the name "piezoelectricity" based on the Greek-derived *piezein*, meaning "to squeeze" [24]. In 1881, Nobel Prize winner Gabriel Lippmann used the fundamentals of thermodynamics to derive mathematical expressions that helped him formulate a prediction he named the "converse piezoelectric effect": the development of a mechanical stress in response to an electrical charge. The Curie brothers quickly confirmed this prediction and proved that the coefficients in each of the mathematical models describing the direct and converse piezoelectric effects were, in fact, one and the same [24]. The efforts of Lord Kelvin, Pierre-Maurice-Marie Duhem, Frederich Pockels, and Woldemar Voigt developed the laboratory curiosity demonstrated by the Curies into an emerging field of science before the end of the 1800's [24].

Today we know that the piezoelectric effect that Jacque and Pierre Curie were able to demonstrate using Rochelle Salt results from the inherent polarity the material derives from its crystalline structure. By the end of 1940's, scientists and engineers discovered that such a polarity need not be inherent to a material's structure but that this property could be macroscopically induced in originally isotropic polycrystalline material by application of an electric field [15]. The process by which this is done is analogous to the magnetization of a permanent magnet and was thus termed "poling." Figure 2.1 provides an illustration of the direct and converse piezoelectric effects [1].

While a number of naturally occurring crystalline materials possess the ability to function as active elements in piezoelectric based devices, many applications that look to exploit this phenomena call for the higher electro-mechanical coupling coefficients found in ferroelectric ceramics. Materials such as Lead Titanate ($PbTiO_3$), Lead Zirconium Titante (PZT), and Lead Lanthanum Zirconate Titanate (PLZT) have substantially higher piezoelectric coefficients than naturally occurring materials [15]. Advanced piezoelectric materials such as these can be obtained in several forms including disk, plates, and rings, as well as custom molded designs from commercial vendors such as Morgan Matroc Inc., Kinetic Ceramics Inc., Piezo Systems Inc., and many others. Even the advanced compositions and geometries offered by the suppliers listed, however, can fall short of meeting the force and displacement requirements called for in certain applications. In order to achieve the requirements imposed by applications such as dynamic system control and precision positioning, a number of ingenious methods have been proposed for amplifying the response of piezoelectric materials.

On of the most commonly employed amplification schemes is the bender actuator. Devices like the bimorph, first introduced by Sawyer in 1931, employed this style of architecture even before researchers had discovered the possibility of inducing polarization in ferroelectric ceramics [25]. Bimorph style benders consist of two ceramic elements adhered together and driven under opposing electrical fields. This can be accomplished employing one of two different configurations. In what is termed the series arrangement, the two elements are bonded together such that they have opposing directions of polarization, and the electric voltage is applied across the thickness of the resulting composite. In the parallel configuration, the two elements are bonded together with similar polarization direction, and the driving voltage is applied to an electrode at the bonding interface. In both configurations the driving voltage results in the simultaneous expansion and contraction of the opposing ceramic plates producing a bending deflection. While the performance of these devices remained poorly understood for almost fifty years, investigations by Steel et al. and Tzou have demonstrated the experimental, theoretical, and applicable knowledge of the concepts governing these devices.

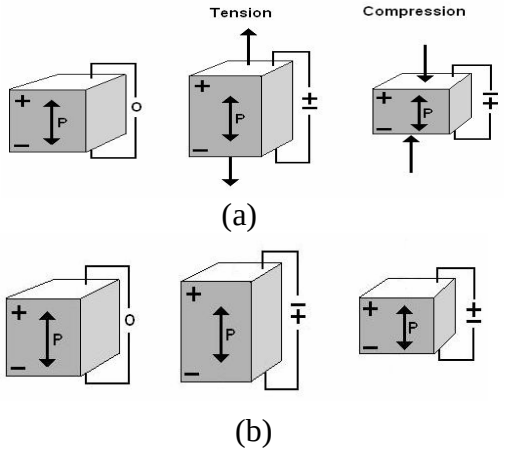

Figure 2.1. The direct, (a), and converse, (b), piezoelectric effects [1].

Unimorph devices are similar in nature to their fellow bimorph benders, but instead of using two ceramics driven in opposing configurations to produce a bending deflection, the unimorph uses only one element adhered to an elastic shim. When the piezoelectric layer of the composite is activated, the expansions and contractions of the element are resisted by the shim and an out of plane deflection results. Commercially available unimorph and bimorph configurations are capable of achieving maximum displacements of several hundred micrometers and generating forces on the order of one Newton [26].

Another amplifying architecture frequently used consists of a linear array of thin ceramics stacked on top of each other. Due to the stacking of ceramics utilized in this scheme, such architecture is commonly referred to as stack actuators. By utilizing several thin ceramics, designers are able to create a device that operates at low voltages. Stack actuators are able to produce increased displacements when compared with single layer ceramics due to the combined contribution of each thin ceramics' displacement. The displacement and force created by these devices are directly proportional to the cross sectional area and length, respectively [27].

Stack actuators were introduced following the discovery of high-strain piezoceramics [28]. Since their advent, piezoelectric stacks have been investigated for a number of applications in the areas of vibration and control applications. While piezoelectric stacks offer many advantages including low voltage operation and high resonance frequencies, the large capacitance of these devices can result in high levels of

power consumption when operated at high frequency. Another drawback inherent in the design of stack actuators is the limited tensile strengths that arise from the laminate construction technique. The stack actuator design has been investigated for independent use as well as being used as an input device for use with other amplifying scheme [27].

An amplification architecture that is capable of utilizing a multilayer stack or piezoelectric ceramic disk is the metal-ceramic composite "Moonie" [29]. The Moonie actuator is a flexural-style actuator developed at Penn State University in the early 90s by Xu [30]. The name "Moonie" is derived from the moon-shaped spaces that are seen between the actuator's flexural housing and the piezoelectric element which resides within [31]. These devices are capable of generating displacements on the order of 100 μm, and forces of up to 10Kg [32]. It has been shown, however, that the force and displacement responses of these devices are highly related to the radius of the active element [29]. A schematic of a Moonie device is shown in Figure 2.2 [29].

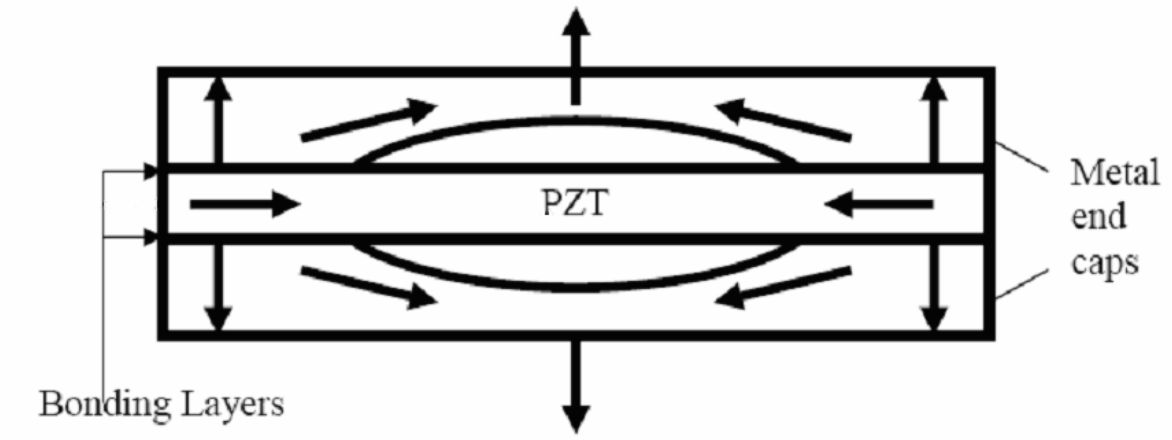

Figure 2.2 Moonie Actuator with arrows showing the direction of motion [29].

While flextensional style actuators like Moonie make effective use of complaint structures to amplify displacement and force, the flexural housings used in this style of architecture can contribute significantly to the system's mass. This added weight may not pose a significant restriction on use of the device for many applications, but it could preclude it from being utilized in the field of aviation, where the system's total mass is of critical importance [33].

Two methods that have proven successful in enhancing the actuation and energy harvesting capabilities of elemental piezoelectric material are the inclusion of a substrate and the application of a prestress [34, 35]. Both of these methods are utilized in Reduced And INternally Biased Oxide Wafers or, RAINBOW^{TM}. Introduced in 1997, RAINBOW^{TM} style actuators use a thermal processing documented in the literature to render one side of a lanthanum zirconium titanate (PLZT) ceramic inactive. The resulting inactive portion of the wafer functions much like the metal shim utilized in Unimorph devices. However, due to a mismatch in the coefficients of thermal expansion found in the two sections of the wafer, the device develops internal thermal stresses which result in a domed form. This domed from produces a compressive pre-stress within the ceramic which enhances piezoelectric performance and protects the ceramic from developing excessive tensile stress during operation [34, 36, 37]. RAINBOW^{TM} actuators were produced by Aura Ceramics Inc.; however, production of the devices has been discontinued [27].

While the development of a compressive thermal stress in RAINBOW^{TM} style actuators offers great improvements over traditional unimorphs, it was not the first actuator

to incorporate this feature. THin layer Unimorph DrivER and sensor, or Thunder® actuators were developed at NASA Langley Research Center 1994 and are currently distributed by FACE International. Like RAINBOW™, these devices rely on a mismatch between the thermal properties of the constitutive layers of the composite to produce an out of plane displacement resulting from the internal thermal stresses introduced in the device during processing. Thunder® devices consist of an elastic substrate, piezoelectric ceramic, and often a protective layer of knurled aluminum adhered with a soluble polyimide developed at NASA Langley Research Center [38]. A schematic of a typical Thunder® configuration is shown in Figure 2.3.

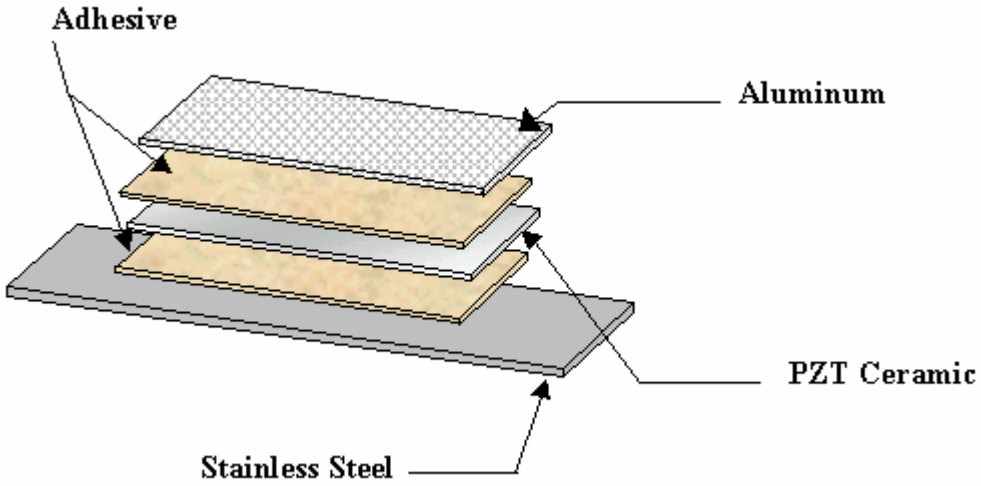

Figure 2.3. Thunder® layering sequence.

The manufacturing process and performance characteristics of Thunder® have been well documented in the literature by a number of research groups [32, 34, 38-41]. Thunder® devices have been investigated for applications such as structural control, energy harvesting, water propulsion, robotics, flow control, and acoustical control, to name a few.

[42-51]. Extensive analysis has been conducted regarding the thermal forces introduced in the device as a result of consolidating constitutive layers with various coefficients of thermal expansion at elevated temperatures [34, 52]. The effect these thermally induced forces have on device performance has been presented [53, 54]. While these devices have been found to produce displacements on the order of several millimeters and forces greater than 4.5 Newtons, there are inherent limitations on optimization of the design due to the coupling that exists between geometrical parameters such as layer thickness and post-manufacturing form, e.g. radius of curvature [55, 56].

Given the wealth of information compiled on prestressed actuators following the introduction of Thunder®, a natural progression of the technology was sure to lead to refinements of concept. One such follow up to the Thunder® concept comes from a research group at Konkuk University in Seoul South Korea. Utilizing the same concepts on which Thunder® is based, researchers at Konkuk have developed a device which replaces the metallic and soluble polyimide layers found in the Thunder® device with prepreg fiber composites. The resulting device is referred to as a LIght weight Piezoelectric Composite Actuator or, LIPCA [33]. Several configurations of LIPCA have been presented, and a detailed account of these devices, and their manufacturing process, has been presented in the literature [55]. A schematic of a typical LIPCA device is shown in Figure 2.4.

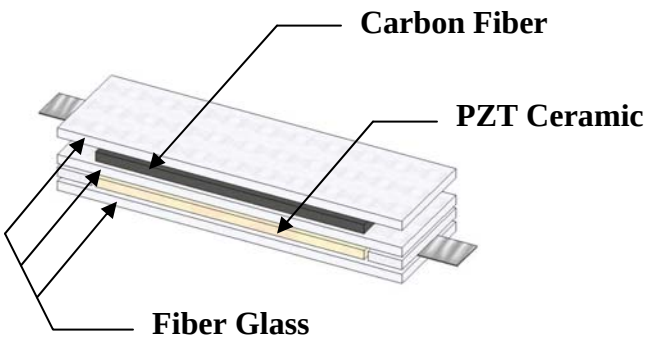

Figure 2.4. LIPCA layering sequence.

By utilizing fiber composites rather than a metal substrate, LIPCA devices are lighter and capable of producing greater displacements than Thunder® devices. [55] Work by Aimmanee has shown that, by utilizing various fiber materials and layering configurations, the neutral axis in LIPCA can be shifted [57]. This quality allows the device to be optimized for use in various applications [33].

While LIPCA has been investigated by many of the same research groups that have evaluated Thunder® devices, LIPCA still lacks the commercial manufacturing methods that have been developed for the Thunder® devices. Other deterrents to widespread use arise from the materials used in LIPCA device. When compared with the stainless steel elements typically used to construct Thunder® devices, the carbon and Kevlar fibers found in typical LIPCA devices result in a dramatic increase in material cost.

2.3 Challenges in Unimorph Design

As previously stated, two methods that have proven successful in enhancing the actuation and energy harvesting capabilities of elemental piezoelectric materials are, one,

the inclusion of substrate, and, two, the application of a prestress [34, 35]. The joining of a piezoelectric element and a flat substrate offer enhanced performance when compared to bare piezoelectric elements, but these simple composites are often unable to outperform effectively designed prestressed piezoelectric unimorphs [27, 58]. The thermally processed, prestressed piezoelectric designs that have been documented in the literature are capable of achieving larger displacements, generating greater forces, and converting energy more efficiently than their simpler composite counterparts. While such devices may offer many favorable characteristics, the disadvantages associated with these devices, which also arise from the requirement of thermal processing techniques, should not be overlooked [39, 59].

Ochinero and Hyer have discussed many of the problems that can arise in the manufacturing of thermally-prestressed curved composite panels [60]. In their work, they identified distortions that can occur in such composites due to non-uniform matrix dispersion, off angle ply alignment, and through thickness expansion. Given the hand lay-up process used to construct LIPCA, and the discontinuity introduced at the site of lead attachments, it is easy to imagine how all three of these issues could be prevalent in a LIPCA device. Many of the troublesome effects that can be found in LIPCA due to its present manufacturing techniques are absent from Thunder® devices due to the commercial manufacturing techniques utilized. If manufacturing processes developed for Thunder® are not strictly adhered to, however, problems are sure to arise. An example of one such complication is demonstrated by the presence of resin-rich regions within the composite

that can result from the viscous flow of the polyamide adhesive during phase transformation.

Even in the absence of the defects identified by Ochinero and Hyer, thermally prestressed actuators still suffer from undesirable limitations arising from their manufacturing. Often these devices are found to utilize soft PZT compositions due to the inexpensive commercial availability of these materials and advanced processing techniques required in the effective re-poling of hard compositions. The use of soft composition piezo-ceramics results in devices that possess limited frequency ranges and piezoelectric properties that show strong temperature dependency. Further disadvantages are inherent in the reduced product lifespan associated with ceramic repoling and the increased manufacturing costs such processes entail.

In order to capitalize on the beneficial characteristics of thermally prestressed devices, while mitigating the negative effects associated with the thermal processing, a designer must develop alternative methods for replicating the characteristic curved form of a thermally processed unimorph. While mechanically prestressing an initially flat unimorph may seem like an easy method for producing the curved form, the tensile fracture limits of the ceramic prevent such a composite from realizing the plastic deformation needed to effectively change the shape of the device. Instead, the present investigation proposes that a substrate be plastically deformed to a desired rate of curvature, after which time a piezoelectric ceramic can be elastically deformed and adhered to the substrate. Eliminating the need to utilize a thermal process to induce the prestressed form removes the coupling between material selection and device form which

currently limits the design of thermally prestressed unimorphs. By replacing such a mechanism with a method of mechanically manipulating the form of a device, researchers provide themselves with a greater range of design space and open the door to a whole new realm of device configurations.

2.4 Summary

This chapter introduced the field of smart materials and provided examples of several commonly utilized smart materials and the applications in which they are implemented. A historical overview of the developments found in the field of piezoelectricity was presented along with factors motivating the use of piezoelectric devices. The chronological progressions of unimorph capabilities were documented and the strengths and weaknesses of current unimorph technologies identified. It is noted that manufacturing processes utilized in the construction of these devices is responsible for both the strengths and weaknesses currently found in unimorphs. A method for constructing a unimorph device, which looks to retain the advantageous effects of thermally processing while mitigating the negative consequences of the process, was postulated. In the following chapter, an analytical treatment of the postulated design is developed, and limitations are determined regarding the design space of a device created utilizing the manufacturing techniques called for by the proposal.

CHAPTER 3

Analytical and Empirical Development of MPC Design

In order to produce a device that functions well in theory and in practice, an analytical model was developed to provide insight into limiting design variables. The model was developed based on the desired final form of the device and stress analysis techniques that have been proven valid for plate geometries. Results from the model were experimentally verified and the limitations identified by the model were taken under consideration before a finalized design configuration was specified.

3.1 Design Considerations

In order to design a device that minimizes radius of curvature without producing a bending moment that results in fracture of the ceramic, the radius of curvature of the composite must be carefully determined. The substrate curvature should be chosen such that it does not allow the radius of curvature of the ceramic to fall below that which would induce tensile fracture in the ceramic. With this limitation in mind, beam theory for a composite structure, allows for the development of elegant moment-curvature and moment-stress relations which can be evaluated to determine the theoretical minimum value of the radius of curvature expected to initiate failure.

At this time it should be pointed out that since the substrate utilized in the present design will be deformed to a desired radius of curvature prior to the application of the adhesive and ceramic, any reference made to the “composite” with regard to the calculations presented in this section is referring to a composite consisting of the ceramic and adhesive only. This assumption allows us to treat the substrate as a fixed structure or form which we are using to define the deformed shape of our adhesive and ceramic composite. While it is clear that the substrate is not a rigid, immovable structure, the results will show that this assumption is in fact valid. Results derived using these assumptions, and evaluation of the defining expressions of beam theory, are experimentally verified. The information gleaned from the analytical framework and empirical results are then used to arrive at the final design configuration.

3.2 Defining Equations

In the present investigation, the flexural formula was used to define the relationship between radius of curvature, bending moment, and the resulting tensile stress. Introductory mechanics of materials confirms the validity of using this methodology based on the length to width ratio of the materials utilized in the study. Use of the flexural formula implies that simple-beam theory for pure elastic bending is applicable, as are the assumptions inherent in the development of this theory. These assumptions state: (a) all sections that are initially plane and perpendicular to the axis of the beam remain plane and perpendicular to it after bending; (b) all longitudinal elements bend into concentric circular arcs; and (c) a one-dimensional stress state is assumed, and the same stress-strain

relationship is used for tension and compression. Figure 3.1 a-c illustrates the stress and strain distribution as well as the internal force and moment generated within a member experiencing loads that meet these criteria [61].

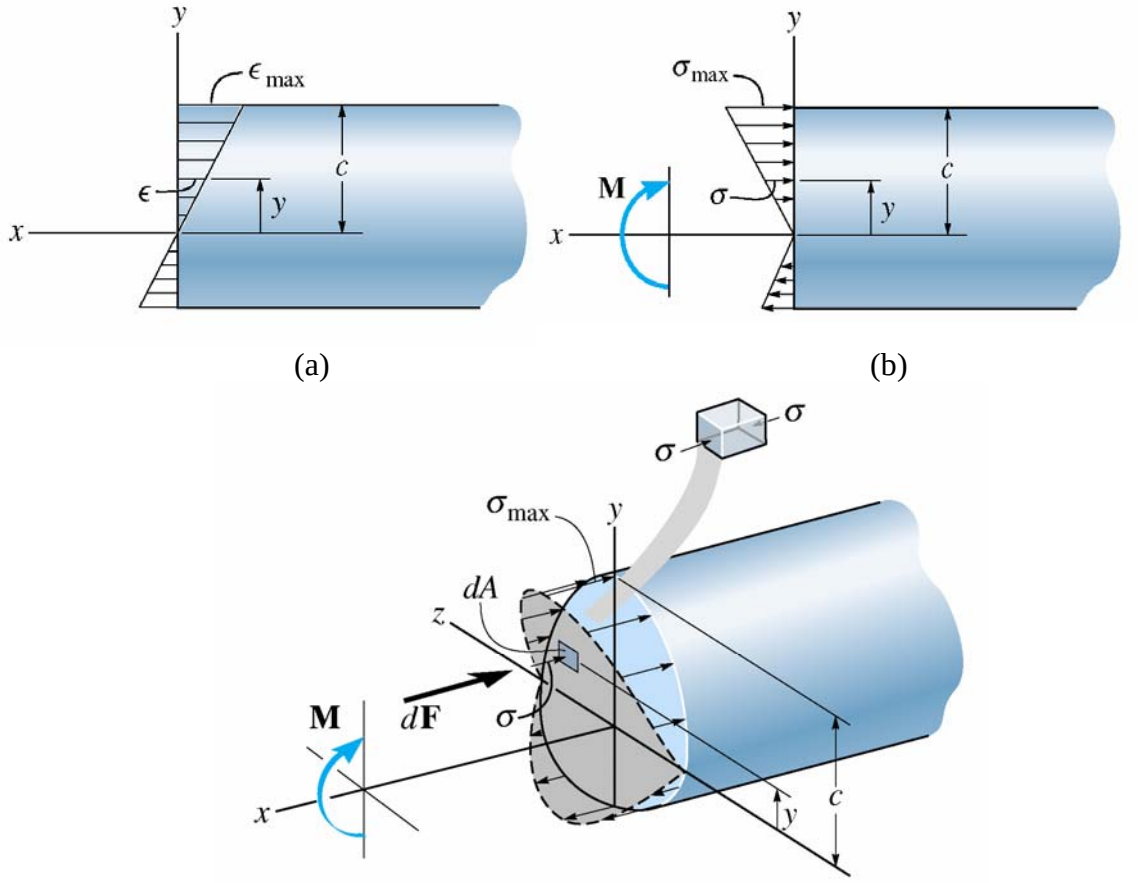

Figure 3.1. (a) Normal strain distribution, (b) Normal stress distribution, and (c) Bending stress variation [61]

The assumption that all sections that are initially plane and perpendicular to the axis of the beam remain plane and perpendicular after bending implies a linear distribution for fiber elongations and contractions. The engineering strain distribution that results from a linear distribution of elongations and contractions is given by Equation 3.1.

$$\varepsilon_x = -\frac{y}{R_n} \qquad \text{Equation 3.1}$$

where R_n is the radius of curvature of the neutral axis and *y* is the distance from the neutral axis. For a linear elastic material, the relationship between axial strain and the applied normal stress can be found as shown in Equation 3.2a through c.

$$\varepsilon_x = \frac{1}{E}\left[\sigma_x - \nu\left(\sigma_y + \sigma_z\right)\right] \qquad \text{Equation 3.2a}$$

$$\varepsilon_y = \frac{1}{E}\left[\sigma_y - \nu\left(\sigma_x + \sigma_z\right)\right] \qquad \text{Equation 3.2b}$$

$$\varepsilon_z = \frac{1}{E}\left[\sigma_z - \nu\left(\sigma_y + \sigma_x\right)\right] \qquad \text{Equation 3.2c}$$

where *E* is Young's modulus and ν is Poisson's ratio. The third assumption specified by beam theory for elastic bending states that $\sigma_y = \sigma_z = 0$. Therefore:

$$\sigma_x = -E\frac{y}{R_n} \qquad \text{Equation 3.3}$$

when Equation 3.3 is combined with Equations 3.2b and 3.2c, the following strain-curvature relations are produced.

$$\varepsilon_z = \varepsilon_y = \nu\frac{y}{R_n} \qquad \text{Equation 3.4}$$

The location of the neutral axis, or the axis of zero stress, is determined from the condition of zero axial forces acting on the beam. Therefore:

$$\int_A \sigma_x dA = -\frac{E}{R_n}\int_A y dA = 0 \qquad \text{Equation 3.5}$$

where *A* is the cross sectional area. Equation 3.5 indicates that the first moment of the cross-sectional area about the neutral axis is zero. This implies that the neutral axis and the centroidal axis are coincident.

The moment-curvature and moment-stress relationships can then be determined from the requirement that the resultant internal moment *M* must be equal to the moment produced by the stress distribution about the neutral axis. From Figure 3.1(c) it can be seen that the moment created about the neutral axis by the differential force element, *d***F,** can be defined as $dM = y\, d\mathbf{F}$**.** Since $d\mathbf{F} = \sigma\ d$A, the sum of moments about the neutral axis gives us an expression for the resultant moment as found in Equation 3.6.

$$M = -\int_A (\sigma_x dA) y \qquad \text{Equation 3.6}$$

Combining Equations 3.5-3.6 and simplifying results in the moment-curvature relationship given by Equation 3.7.

$$R_n = \frac{E}{M} I_z \qquad \text{Equation 3.7}$$

And the moment-stress relationship is expressed by Equation 3.8.

$$\sigma_x = -\frac{M \cdot y}{I_z} \qquad \text{Equation 3.8}$$

The equations presented above define the state of stress resulting from a given radius of curvature. A comprehensive summary of the evaluation and experimental verification of the results provided by these relationships is presented in the next section.

3.3 Theoretical Design Limitations

An elementary knowledge of the structure of ceramics reveals that tensile stress is the most likely cause of failure. The increased propensity of tensile induced fracture in ceramics can be largely attributed to the nature of the ionic bonds exhibited within these materials. The likelihood of tensile fracture is amplified by the ease with which stress concentration can develop within these porous materials and the diminished number of slip systems available in crystalline structures. The increased porosity of any material often results in inconsistencies in the values found for mechanical properties due to variations in the magnitude of stress concentrations that develop at cavities within the material. All of these factors must be considered when trying to reconcile design limitations obtained from theoretical and experimental methods.

Work done by Guillion et al., 2002, shows that, for soft ceramic compositions such as PZT 5A, ultimate tensile strength values have a range of 25-35MPa [62]. The value of Young's modulus for the ceramics used in the present investigation was provided by the manufacturer as 69GPa and values for the modulus of the acrylic pressure sensitive adhesive were assumed to range between 13.5-24 kPa [63]. Rearranging Equation 2.3 and substituting in values of the pertinent parameters gives a range of values for the magnitude of curvature that is expected to result in tensile failure. The calculations used to determine this range of values are presented below in Equation 3.9.

$$R_n = -E_{eff}\frac{y}{\sigma_u} \qquad \text{Equation 3.9}$$

Where *y* is the distance from the mid-plane of the adhesive-ceramic composite to the upper surface of the ceramic, σ_u is the ultimate tensile strength of the ceramic, and E_{eff} is the effective modulus of the composite as defined by the rule of mixtures, shown by Equation 3.10:

$$E_{eff} = V_A \cdot E_A + V_C \cdot E_C \qquad \text{Equation 3.10}$$

Where V_A and V_C represent the volume of the adhesive and the volume of the composite, respectively. And, E_A and E_C represent the elastic modulus of the adhesive and ceramic, respectively. Utilizing the range of ultimate tensile strength values presented by Guillion, 25MPa to 35MPa, the minimum radius of curvature obtainable is found to lie between 13.63cm and 19.08cm. These values represent the theoretical limits on the curvature of a device constructed using PZT 5A and the given adhesives, with their specified dimensions. To validate these calculations, an experimental procedure was developed. Details of this procedure, and the results of the testing carried out subsequently, are presented in the following section.

3.4 Experimental Design Verification

To validate the limitations on curvature developed in the preceding section, an experimental test fixture was developed. The fixture allowed for the curvature of a substrate to be continuously modified so that the magnitude of curvature which results in the tensile fracture of a ceramic element could be determined. This fixture consists of two aluminum blocks measuring 5cm by 5cm by 20cm long, a steel plate measuring 0.135cm

thick by 20cm wide by 30cm long, an optical table, and an adjustable optical stage. A schematic of the test fixture is shown in Figure 3.2.

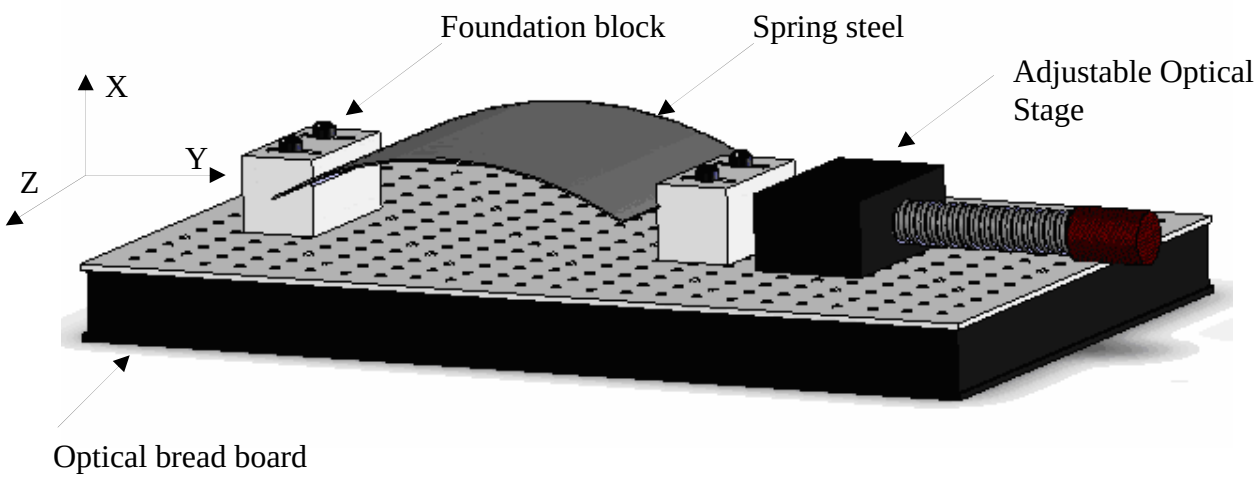

Figure 3.2. Adjustable radius fixture.

When configured in the arrangement shown in Figure 3.2, an extension of the jack results in a decrease in the radius of the steel plate. To determine the curvature at which tensile failure is eminent, a piece of Kapton film was used to hold adhesive-ceramic composite samples against the substrate while the radius of the plate was decreased until facture occurred. The radius of curvature of the substrate was then calculated using Equation 3.11 [32].

$$r = \frac{h}{2} + \frac{S^2}{8h} \qquad \text{Equation 3.11}$$

Where h and S are measured as shown in Figure 3.3.

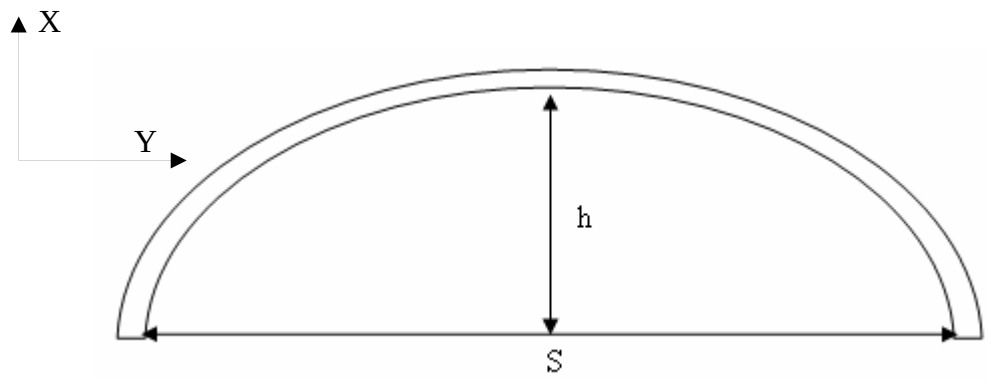

Figure 3.3 Schematic representation of dome height and footprint dimensions

With the radius of curvature of the substrate known, the radius of curvature of the ceramic could then be determined. Values of the magnitude of curvature that were found to incite failure were recorded and saved for later analysis. The average value of the radius found to incite failure in the ceramic was found to be 13.13cm.

3.5 MPC Design Specification

An analytical formulation was used to define the relationship between device curvature and ceramic stress. This formulation allowed researchers to determine the theoretical limitations on the curvature of the device and experimental efforts were undertaken to verify the accuracy of the results. These efforts found that ceramics were theoretically expected to experience tensile fracture when deformed to a radius between 13.63cm and 19.08cm. Efforts undertaken to experimentally verify these results showed reasonable agreement with the theoretical predictions. An average radius of 13.13cm was experimentally determined to be the magnitude of curvature which results in tensile

fracture for ceramics measuring 7.62 x 4.45 x .018 cm. This value represents the minimum radius to which a device can be constructed without being expected to fracture.

Given that the application of an AC field results in both increasing and decreasing the curvature of a prestressed unimorph, the curvature of the device was chosen such that failure would not be achieved during application of a driving field. To ensure that the present class of devices did not experience failure during driving conditions, the radius of curvature of the substrate was chosen slightly larger than that found to experimentally induce fracture, that value being 14cm. With the radius of curvature of the stainless steel substrate chosen, the final device configuration was defined. The final form of the device consisted of the deformed substrate adhered to a PZT plate using a commercially available pressure sensitive adhesive. An upper covering of Kapton film was used to apply the deforming force to the ceramic while having the added benefit of acting as a translucent protective cover, allowing for visual inspection of the device.

While Kapton film was used in the present investigation, it is acknowledged that any translucent film strong enough to provide the force necessary to deform the ceramic could be used in construction of future devices. It should also be noted that other material could also be used as an elastic substrate. However, in the present investigation, stainless steel was used to facilitate greater fidelity in the comparison to existing devices. It also offered the added benefit of providing a rigid, corrosion resistant platform, which adheres well to the pressure sensitive tapes implemented.

3.6 Summary

This chapter introduced an analytically based model that was used to assess the theoretical limitations imposed on the curvature of an MPC unimorph by the tensile fracture limits of the ceramic. The theoretically derived limits were experimentally verified using equipment and procedures developed at Virginia Commonwealth University. Following the experimental verification of the predicted limits imposed on curvature, a final MPC design configuration was established. Details concerning the manufacturing procedures implemented in the production of the established design are presented in the following chapter.

Chapter 4

Manufacturing Procedures

Mechanically prestressed piezoelectric composites are composed of four elemental components: (1) a base structure, (2) a joining mechanism, (3) a piezoelectric material, and (4) electrical leads. In their most basic configuration, these elements work together to produce a prestressed composite that is similar in nature to thermally prestressed unimorphs. Many of the materials used in the present MFC design were chosen based on their incorporation in Thunder® devices. This was done in an effort to eliminate as many variances between the devices as possible, and thus to allow for a faithful comparison between to methods of prestressing. In the present investigation, the MPC utilized stainless steel 304 as a substrate material. For a piezoelectric element, a soft ceramic, measuring approximately 0.18mm thick, was purchased from Morgan Matroc. Two different pressure sensitive adhesives, obtained from Avery Dennison, were examined as a joining mechanism for use in the composite. Throughout the reminder of the work, the two adhesives, which are sold under the names MS 3032 and FT 2002, will be referred to as Adhesive A and Adhesive B, respectively. Documentation provided by the manufacture regarding the properties of the adhesives can be found in Appendix D. To facilitate electrical connection to the ceramic, 0.00254 by 0.3175cm Nickel wire, obtained from Wiretronic Inc., was utilized.

The manufacturing process of an MPC can be divided into four basic steps. These steps consist of: (1) sample preparation, (2) base structure formation, (3) consolidation of the constitutive layers, and (4) quality assurance. These processes are described in detail in the following sections.

4.1 Substrate Sample Preparation

The substrates used in the investigation were cut from 20.32 by 30.48cm stainless steel shim stock obtained from McMaster-Carr. From the stock plates, samples measuring 4.76 by 9.21cm were rendered using a Calypso Waterjet System Inc. abrasion cutting machine. Water abrasion cutting was utilized to ensure sample dimensionality and to minimize the introduction of superfluous stresses associated with other machining practices. After the samples were cut to the desired dimension, the edges were filed to remove any burs or other undesired artifacts of the cutting process. Before the substrates were deformed to the desired curvature, the surfaces were cleaned and textured using 120 grit sandpaper to promote bonding.

4.2 Substrate Curvature Formation

While an automated hydraulic plate bending roll could be implemented as a cost effective means of obtaining the desired substrate curvature in a commercial manufacturing operation, in the current investigation, the elastic substrate material was formed to a desired radius of curvature via an iterative, hand-formed process. The process

consisted of bending the samples over forms of various diameters, checking the deformed shape against a prefabricated template, and making adjustments as needed. To confirm that the samples had in fact been stressed to the desired curvature, the post-bending radius of curvature of each sample was experimentally determined using Equation 3.11. In an effort to ensure uniformity of curvature amongst the various samples, an ample number of substrates were prepared for each of the given device configurations. From the prepared samples, the eight prestressed substrates most closely matching the desired radius of curvature for each substrate thicknesses to be examined were selected for use in construction of the composites. The experimentally determined radius of curvature for each sample, and the adhesive used with each sample, are shown in table 4.1.

Table 4.1. Substrate's Radius of Curvature and Adhesive Association.

Substrate Thickness	0.10 mm (4 mil)		0.13 mm (5 mil)		0.18 mm (7 mil)		0.25 mm (10 mil)		0.30 mm (12 mil)	
	ID	R_C (cm)	ID	R_C (cm)	ID	R_C (cm)	ID	R_C (cm)	ID	R_C (cm)
Adhesive A	10A	13.37 13.64 13.39 13.67	13A	13.72 13.36 13.01 13.40	18A	13.52 13.30 12.98 13.08	25A	13.20 13.61 13.20 13.08	30A	12.76 13.58 12.88 13.58
Adhesive B	10B	13.73 13.76 12.96 13.42	13B	13.13 13.80 13.22 13.14	18B	13.43 13.93 13.37 13.55	25B	13.35 13.21 13.43 13.44	30B	13.67 13.06 12.89 12.95

4.3 Consolidation of Constitutive Layers

After the radius of curvature of each sample was determined, and substrate samples were associated with a given adhesive, the substrates were cleaned using isopropanol and

lint free towels. The adhesive was then applied by rolling the substrate against the adhesive film along the longitudinal axis of the curved form. To provide uniform adhesion between the pressure sensitive film and the substrate, the materials were then placed in a specially designed pneumatic press, where a uniform pressure of approximately 175 kilopascals was applied to the composite for a period of five minutes. Upon removal from the press, the radius of curvature of each device was once again measured to ensure that the desired dimensionality was not compromised. A schematic of the pneumatic press is shown in Figure 4.1. Following pneumatic consolidation of the substrate and adhesive film, the films poly-coated liner was removed, and a visual inspected allowed for assessment of continuity along the bond interface.

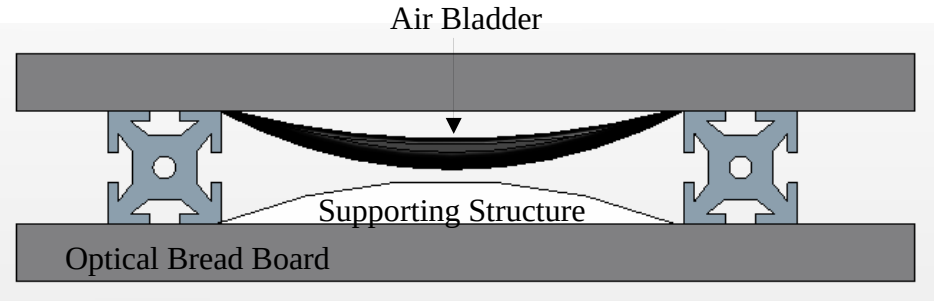

Figure 4.1. Schematic of pneumatic press used in consolidation process.

To provide an uncompromised electrical connection to the surface of the ceramic, a length of Nickel wire, measuring approximately 9cm, was placed atop the adhesive along center the longitudinal axis of the substrate. Before application to the adhesive film, the surfaces of the wire were knurled, and then cleaned using isopropanol and lint free towels.

After leads were attached to the metal-adhesive composite, attention was turned to consolidation of the ceramic. Markings placed at the center of the longitudinal and transverse edges of the ceramic and substrate aided in proper alignment of the composite's layers. During consolidation of the ceramic, the substrate structure was placed on a fabricated support to prevent deformation. The markings on the substrate and ceramic were aligned by sight as the ceramic was rested on the apex of the curved composite. The final resting arrangement achieved by this process is shown in Figure 4.2.

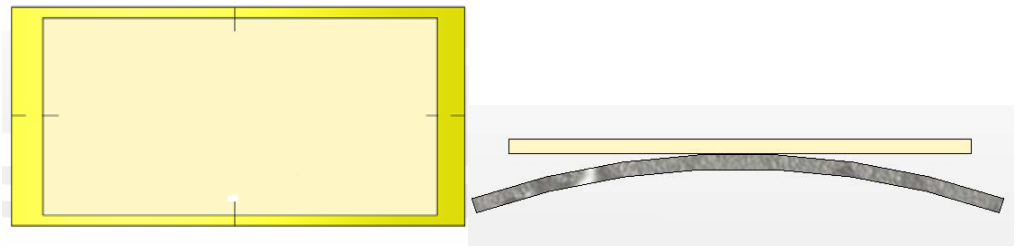

(a) (b)

Figure 4.2. (a) Top and (b) front views of base and ceramic alignment.

In order to deform the ceramic to desired radius of curvature without applying an excessive bending moment, a piece of Kapton film was held taut, parallel to the surface of the ceramic, and the film was then gradually lowered in order to apply a uniformly distributed load to the surface area of the PZT. Once the Kapton film was lowered to a position that resulted in full contact between the ceramic and the base structure, pressure was applied along the edges of the device to promote adhesion between the pressure sensitive film and the Kapton film. This was done to help prevent the edges of the ceramic

from delaminating as a result of the internal stress introduced in the material. To ensure quality consolidation of the composite, the device was once again placed in the pneumatic press where a pressure of approximately 175 kilopascals was applied for a period of five minutes.

4.4 Quality Assurance

After the devices were constructed, visual and electrical inspections were undertaken to ensure the quality of the composite. The surface of each device was visually inspected and post manufacturing capacitance values were compared with capacitance values taken of the bare ceramics to determine if the PZT had developed any cracks during the deformation process. Digital calipers were used to investigate any variations in the thickness of the composite that may allude to areas of delamination. Of the forty devices that were constructed for the current investigation, all forty were found to be free of defect upon completion of the manufacturing process.

4.5 Summary

This chapter revealed the manufacturing procedure utilized in the construction of the newly proposed unimorph devices. The techniques implemented to promote effective adhesion were disclosed along with the methods used to ensure uniform consolidation. Schematics of the consolidating press utilized in manufacturing process were presented. The chapter concluded with a discussion of the measures that were taken to ensure that a quality composite was produced.

Chapter 5

Performance Evaluation: Test Equipment and Procedures

All experiments were conducted at Virginia Commonwealth University's Smart Materials Lab. High resolution photographs of several samples were provided by NASA Langley Research Center. A description of the experimental setups implemented in the investigation, along with detailed information concerning the equipment utilized, is presented in the following sections.

5.1 Laboratory Equipment

The electromechanical characterization of the current class of mechanically prestressed composites was performed in the Smart Materials Lab at the Virginia Commonwealth University, located in Richmond, Virginia. Characterization was undertaken using computer controlled data acquisition systems and equipment. The hardware utilized in the investigation included a desktop computer equipped with a National Instrument SCB-68 I/O connector block, a Hewlett Packard 33120A Function Generator, a TREK PDZ700 Power Supply Amplifier, a NAIS laser displacement sensor, a Stanford Research Systems SR640 Dual Channel Low Pass Filter, a Tektronix TDS 2024 oscilloscope, a Vishay Micro-Measurements P3 Strain Indicator and Recorder, and a

Hewlett-Packard Impedance Analyzer. All applicable hardware was monitored and controlled using LabVIEW^{TM} software. A diagram of the data collection system is shown in Figure 5.1.

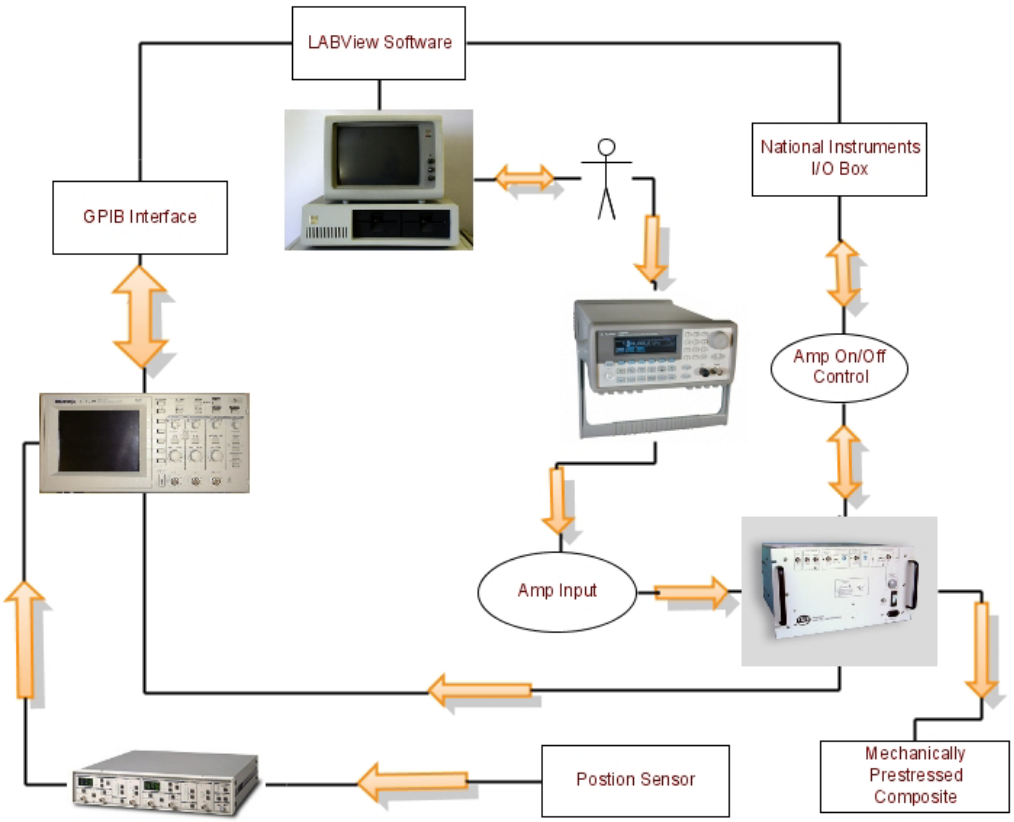

Figure 5.1. Data acquisition system

In the data collection system shown in Figure 5.1, the Hewlett Packard 33120A Function Generator is used to provide the TREK PDZ700 amplifier with the driving signal need for AC and DC operation. The Hewlett Packard 33120A is equipped with a frequency range of $100\mu Hz - 15MHz$ with a resolution of $10\mu Hz$ and an accuracy of 10ppm. The

function generator has an output amplitude range of $50mVpp - 10Vpp$ with an accuracy of $\pm 1\%$ of the specified output.

The Hewlett Packard 33120A was used to drive a TREK PDZ700 power amplifier, which was factory configured with a 1Mohm inverting input and digital enabled TTL control via a BNC connection. The amplifier provides a bipolar voltage range of $0 \pm 700V$, output current capabilities of $\pm 100mA$, and was configured with a gain of $400 V/V$. The on-off operation of the amplifier was controlled via LABView software, interfaced with a National Instrument SCB-68 I/O connector block. The output signal was confirmed using a Tektronix TDS 2024 oscilloscope.

A NAIS LM10-ANR12511 laser displacement sensor was used to measure the center displacement of the present class of devices in response to mechanical and electrical loading. The NAIS LM10 series of laser displacement sensors are optical triangulation measurement devices. The LM10 model ANR12511 used in the present investigation was configured with an ANR5232 pnp controller. The LM10-ANR12511 is a high-power class 2 laser which has a range of $50 \pm 10mm$ and a resolution of $1\mu m$. Output from the ANR5232 pnp controller was routed to a Stanford Research Systems SR640 Dual Channel Low Pass Filter before being routed to a Tektronix oscilloscope for further investigation.

The Tektronix TDS 2024 oscilloscope was used to acquire driving voltage and displacement signals so they could be visually inspected and downloaded to a desktop computer. The Tektronix TDS 2024 is equipped with four input channels, a $2.0 GS/s$ sampling rate, vertical sensitivity of $2mV$ to $5 V/div$, and vertical resolution of 8-

bits. Control of the oscilloscopes settings and signal downloading were accomplished through use of a GPIB interface and LABView software.

The Hewlett Packard 4194A Impedance/Gain-Phase Analyzer was used to measure capacitance and other impedance characteristics as a function of driving frequency. The HP 4194A is capable of making frequency-based measurements with a driving voltage range of 10mV to 1V rms while providing a DC offset of $0 \pm 40V$ and a maximum current output of 0 ± 20 mA. The 4194A can provide these driving voltage and current magnitudes while evaluating 11 different impedance characteristics over a frequency range of 100 Hz to 15 MHz with a resolution of 1 mHz.

5.2 Displacement Measurements

To establish a comprehensive understanding of the electro-mechanical response of the present class of devices, center displacement measurements were obtained for mechanical, electrical, and combined loadings. In all cases displacements were evaluated while the device was supported by a specially designed test fixture that was developed and constructed at NASA Langley Research Center in Newport News, Virginia. A schematic of the test fixture is shown in Figure 5.2.

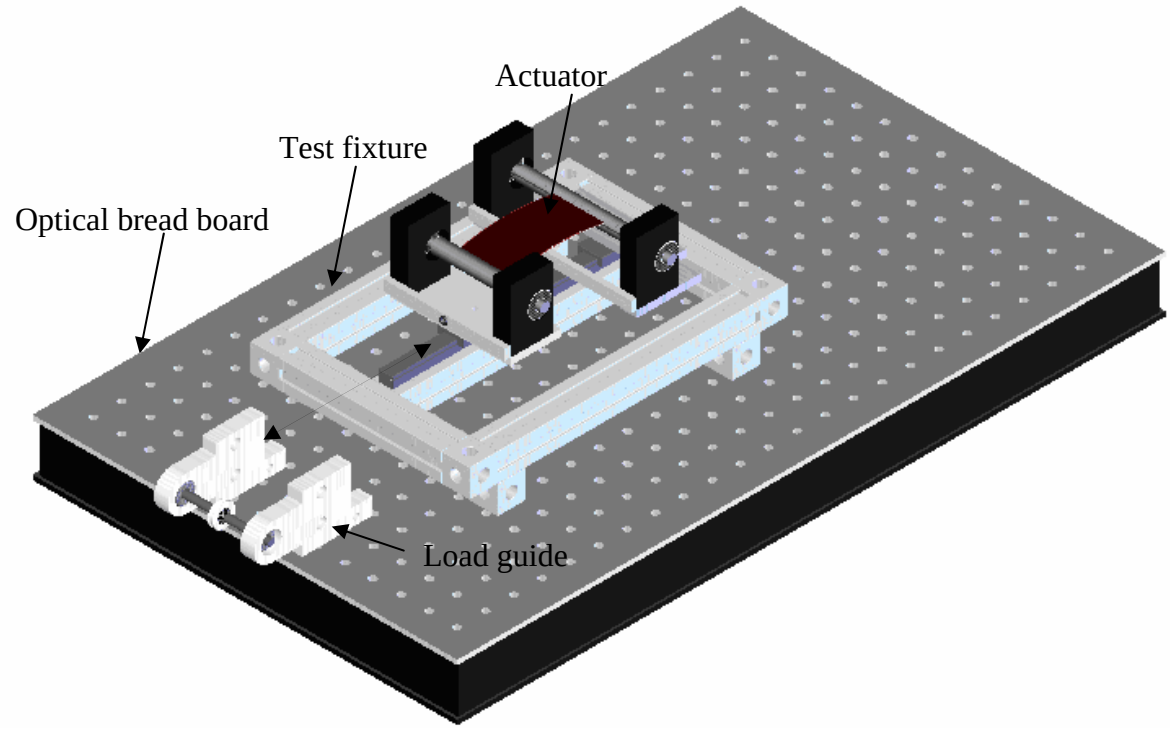

Figure 5.2. Actuator supporting test fixture.

The fixture provides the device with a fixed-free boundary condition which allows for rotation of both ends and translation of the free boundary. Rotation of the attached edges is allowed for by use of ball bearing mounted supports. Translation of the free boundary is facilitated by way of a linear ball bearing assembly to which the actuator supports are mounted. The fixture allows the investigator to select which end of the device will be fixed, which will be free, and to which end the load will be applied. These options allow for both tensile and compressive loading to be accommodated in addition to electrical loads. The fixture ensures that the magnitudes of the mechanical loadings are

uniformly disputed along the end of the device. The loading combinations that were investigated in the present work are shown in Table 5.1.

In the present investigation, mechanical loads were applied in increments of 200 grams. In order to allow for a comparison between MPC performance characteristics and those found in the literature for Thunder® devices, electrical and mechanical loadings were applied over ranges comparable to those used by previous investigations. For the case of mechanical loading, tensile loads were applied in increments of 200 grams over a range of 200 to 1800 grams. In the case of AC electrical loading, the device response was assessed from $50 - 350Vpp$ with measurements taken at 50 volt increments within specified the range. The same resolution was used while determining the DC response, however, voltages were applied over a range of $50 - 350V$ rather than $50 - 350Vpp$.

Table 5.1 Mechanical and electrical load configurations

Loading		
Electrical		Mechanical
AC	DC	Tension
X		
	x	
		X
X		X

The effect of loading was investigated by first looking at the free displacement produced by the device over the applied voltage range. The extreme mechanical-electrical combinations were then documented, followed by a subsequent assessment of the free electrical response. Researchers have shown that excessive mechanical or electrical

loading can result in the depolarization of a ceramic. One manner of assessing whether depolarization from such events has occurred is to closely monitor the performance characteristics of a sample to determine if performance degradation is evident. By comparing results of the free displacement achieved by the devices before and after combined loading investigations were undertaken, it was determined that even the most extreme combined loading configurations did not result in any degradation of the ceramic's polarization. Following this quality assurance procedure, intermediary loadings were assessed.

5.3 Force Measurements

The effective stiffness and blocking force of the device under investigation was determined by analyzing mechanically and electrically induced displacement data. The effective stiffness of the device was determined by calculating the inverse slope of a linear fit of mechanical load versus displacement data. In the current study, blocking force for a given voltage was defined by the tensile load resulting in a ninety percent reduction in displacement over that seen during mechanically free trials. The magnitude of this value was determined by evaluating a linear fit of load versus displacement data. In both cases the data used to calculate the least squares fit was comprised of averaged responses seen for the given loading conditions, for a given device configuration.

5.4 Strain Measurements

Strain measurements were obtained using a Vishay Micro-Measurements P3 Strain Indicator and Recorder and Vishay rosette strain gauges. The rosettes utilized in the investigation were adhered to the top of the ceramic using a commercially available cyanoacrylate adhesive. To promote effective bonding, the surface of the ceramic was prepared as outlined in section 5.2. Strain gauges were connected to the P3 Strain Indicator and Recorder in a quarter bridge arrangement using a 120 Ohm shunt resistance as shown in Figure 5.3. The P3's Min/Max Capture function was utilized to obtain peak values of the tensile and compressive strains induced in the ceramic during mechanical and electrical loading.

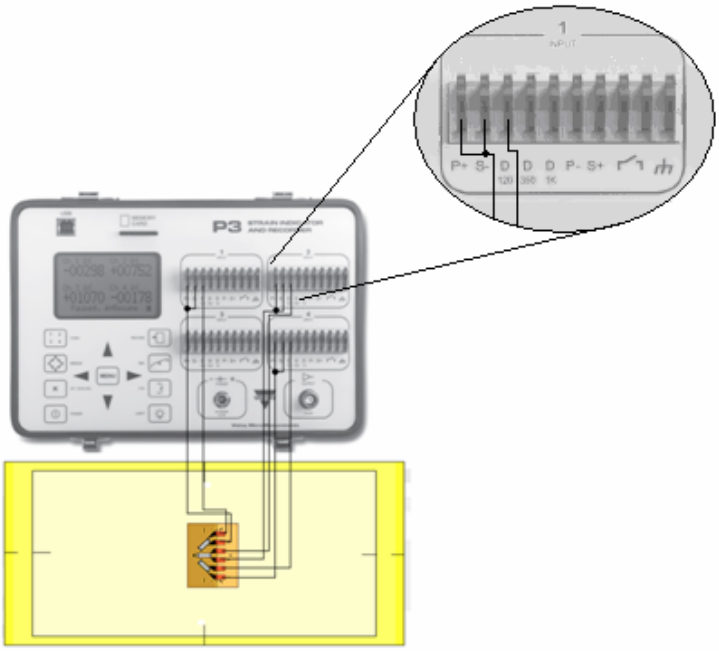

Figure 5.3. Strain data acquisition system and wiring diagram.

The maximum tensile and compressive strains developed in the device were used to calculate the principle strains and their orientation. In the case of mechanical loading, these values were captured approximately 10 seconds after the application of the load. In the case of electrical loading, the maximum displacement and maximum strain are developed and recorded immediately following the application of the field. With the strain gauges oriented as shown in Figure 5.4, the principle strains ε_1 and ε_2,as well as their orientations, as defined by ϕ, can be obtained from Equations 5.1 and 5.2.

$$\varepsilon_1, \varepsilon_2 = \frac{\sigma_x + \sigma_y}{2} \pm \sqrt{\left(\frac{\sigma_x - \sigma_y}{2}\right)^2 + \left(\frac{\tau_{xy}}{2}\right)^2} \qquad \text{Equation 5.1}$$

$$\phi = Tan^{-1}\left(\frac{\tau_{xy}}{\sigma_x - \sigma_y}\right) \qquad \text{Equation 5.2}$$

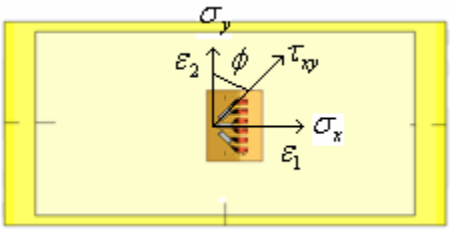

Figure 5.4. Rosette strain gauge placement and principle strain orientation

5.5 Impedance Measurements

Impedance and capacitance measurements were made over a frequency range of 100Hz to 1MHz with samples taken at increments of 1Hz. Measurements of the bare piezoelectric plates were taken by securing leads to stainless steel plates which were then

placed on the upper and lower surfaces of the ceramic. For investigation of the impedance characteristics of the piezoelectric elements utilized, the negative lead of the device was used in conjunction with flat nickel wire and cellophane tape to establish the necessary electrical connections. In both cases, samples were placed on an inflatable structure to isolate vibrations induced in the device during excitation through the given frequency range.

5.6 Summary

This chapter provided detailed information concerning the test equipment used in the performance evaluation of MPC devices. Pertinent evaluation procedures were outlined and meticulous accounts of important equipment settings and specifications were provided. The following chapter presents and discusses the results derived from the efforts outlined in this chapter.

Chapter 6

MPC CHARACTERIZATION

Investigations conducted by Mossi et al., Ounaies et al., Aimmanee et al., and others have demonstrated the large number of variables affecting the performance of prestressed piezoelectric devices [41, 44, 52 , 55]. In order to assess the performance of MPC devices, the present investigation collected data pertaining to dependent variables historically found most influential to the performance of prestressed devices. Work on the characterization of prestressed devices such as Thunder® and LIPCA has been presented by Mossi, Schwartz, and Aimmanee. Investigations conducted by these researchers have demonstrated the importance of material dimensions, layering sequence, driving voltage, and frequency, as well as the magnitude and topology of applied stresses.

In an effort to control the independent variables deemed significant by previous researchers, the specially designed test fixture described in Section 3.2 was used to ensure consistency in the application of mechanical loads and boundary conditions. In all the device configurations investigated, the dimensions of the ceramic were held constant. To further isolate the effects of pertinent independent variables, experiments were conducted using static electric fields, or alternating fields with frequencies of 1Hz. Alternating fields of 1Hz were used to mitigate dynamic effects that could be incited by higher frequency driving conditions. With defined ceramic dimensions, boundary conditions, and driving

frequencies, the remaining independent variables consist of adhesive and substrate dimensions, as well as the range of the mechanical and electrical loadings. Using the loading ranges specified in Section 5.1, this list is further reduced to material geometry alone. With device configurations including two different adhesives, and five different substrate thicknesses, a total of ten unique device configurations were provided. A detailed description of the manufacturing process used to construct four samples for each of the ten different device configurations is included in Chapter 4. A summary of the differences found between these various configurations is provided by Table 6.1.

Table 6.1. Device configurations and their designating notation

Designation	Adhesive	Substrate
10A	MS3032	0.10mm SS
13A	MS3033	0.13mm SS
18A	MS3034	0.18mm SS
25A	MS3035	0.25mm SS
30A	MS3036	0.30mm SS
10B	FT2002	0.10mm SS
13B	FT2003	0.13mm SS
18B	FT2004	0.18mm SS
25B	FT2005	0.25mm SS
30B	FT2006	0.30mm SS

6.1 Displacement-Voltage Profiles

Due to the large amount of data available, the results presented only contain typical displacement trends displayed at prescribed AC and DC voltages. Figures 6.1 through 6.5 show the average peak-to-peak displacements induced by various magnitudes of AC driving voltages. Each graph presents the average response of devices constructed with both Adhesive A and Adhesive B. The trends shown in Figures 6.1-6.5 indicate that for the range of voltages and substrate thicknesses investigated, the voltage induced displacement

decreases as the substrate thickness increases. Such a relationship is intuitive and it is indicative of the responses reported by previous investigations on thermally prestressed devices.

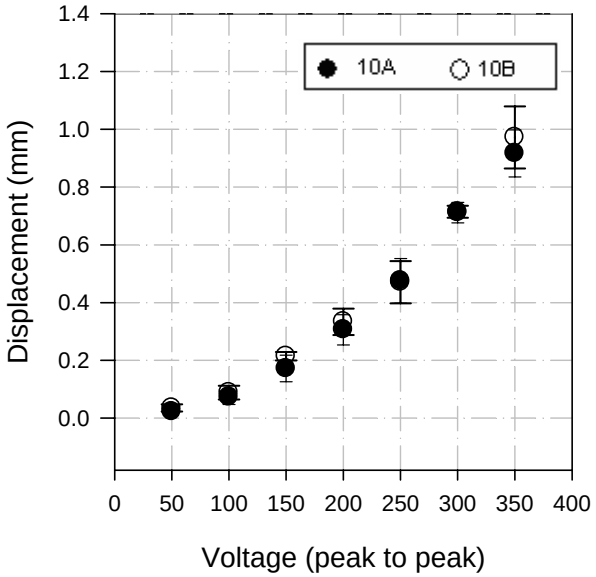

Figure 6.1 Averaged peak-to peak displacement in response to an AC field of configurations 10A and 10B

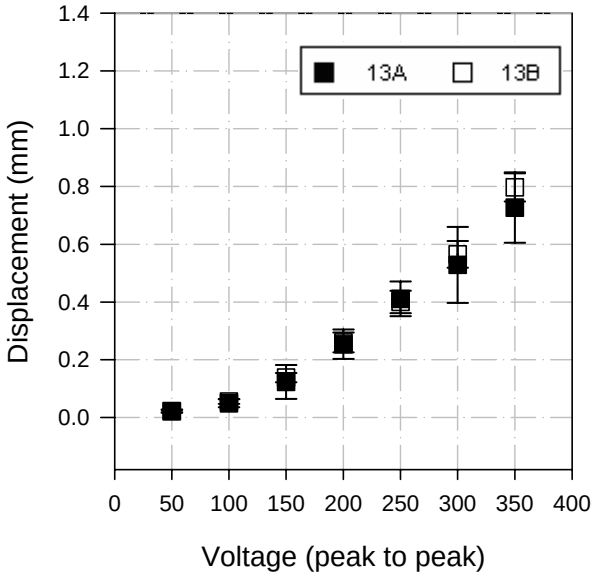

Figures 6.2 Average peak-to peak displacement in response to an AC field of configurations 13A and 13B

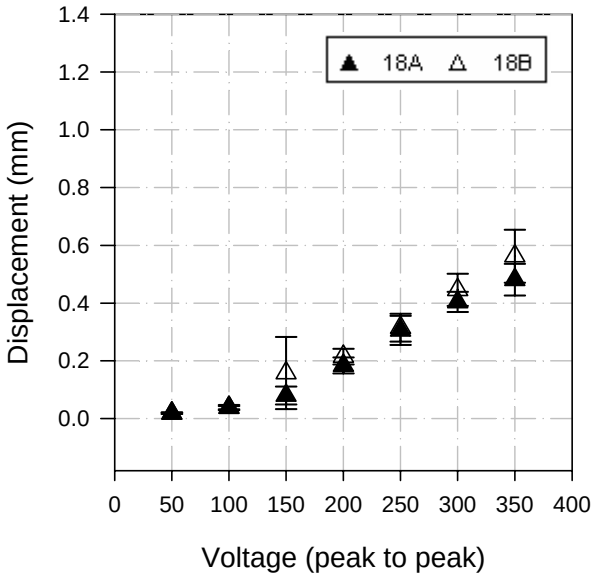

Figures 6.3 Average peak-to peak displacement in response to an AC field of configurations 18A and 18B.

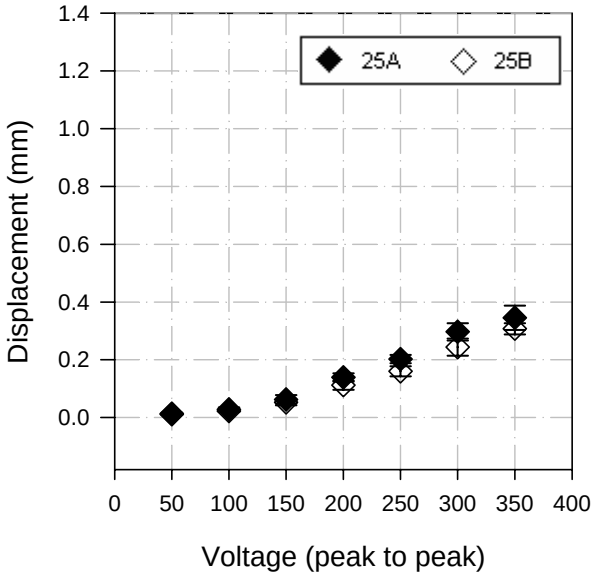

Figures 6.4 Average peak-to peak displacement in response to an AC field of configurations 25A and 25B.

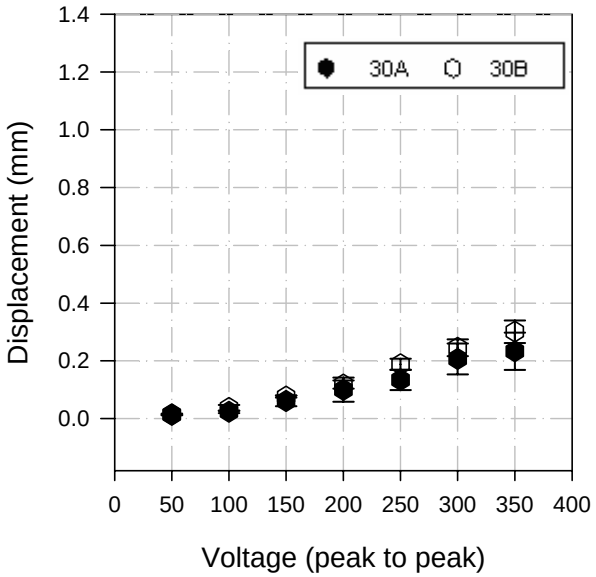

Figures 6.5 Average peak-to peak displacement in response to an AC field of configurations 30A and 30B.

An assesment of the dynamic response of the devices under investigation provided researchers with insight into the mechanical charaicterisitics governing the device. Examining the step response of the actuators, while remaining mindful of the creep-related characteristics usually associtated with peizoelectric materials, suggest that the mechanical properties of the adhesive significantly contribute to the over-damped characteristic of the device. The step responses, presented in Appendix A, show that the maximum displacement of a device can be approxiamtely twenty five percent larger than the steady state DC displacement. In the present investigation, the DC displacement of the device was defined by the steady state displacement so as to provide future researches with an idea of the sustainable displacement that comparable devices are capable of displaying. Figures 6.6-6.10 show the average steady state displacements achieved by the various device configurations in response to a DC driving field over the prescribed range of voltages.

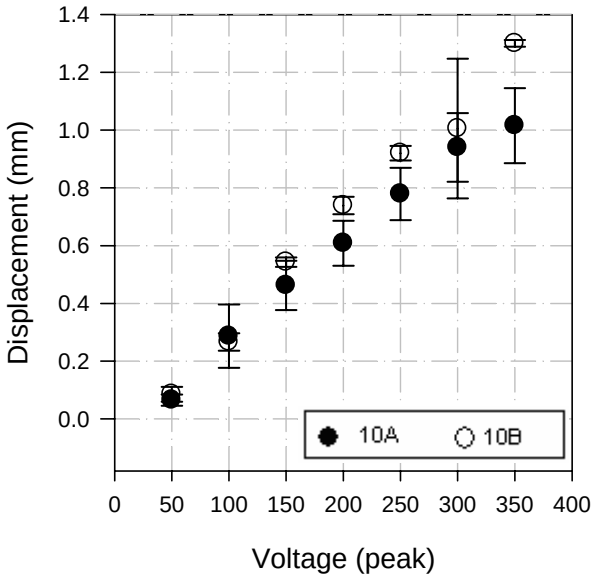

Figures 6.6. Average DC response of configurations 10A and 10B.

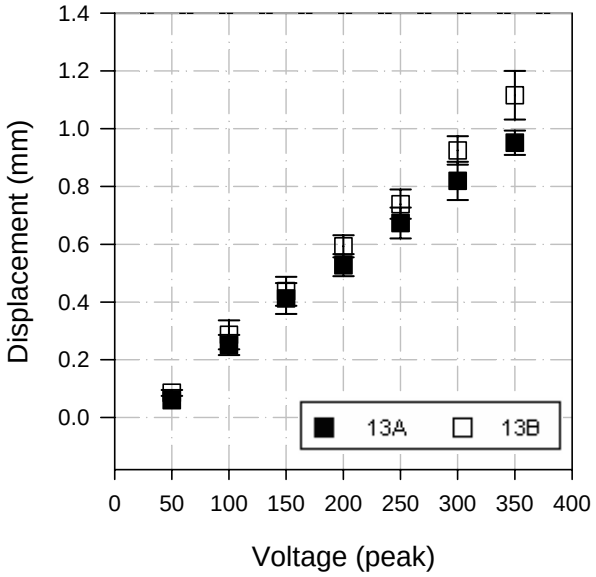

Figures 6.7. Average DC response of configurations 13A and 13B.

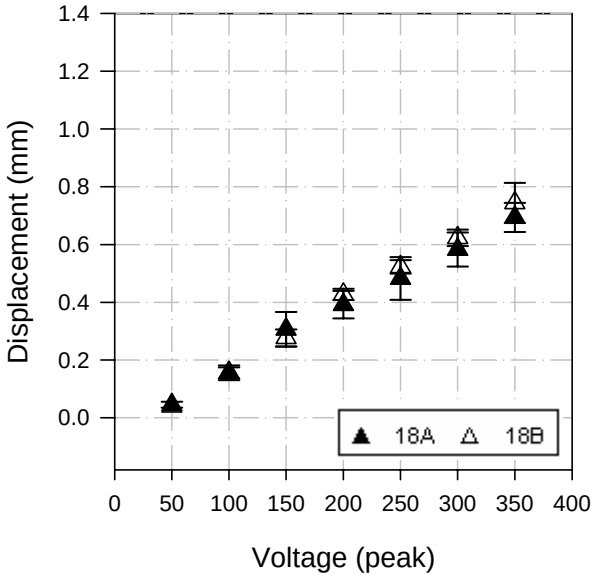

Figures 6.8. Average DC response of configurations 18A and 18B.

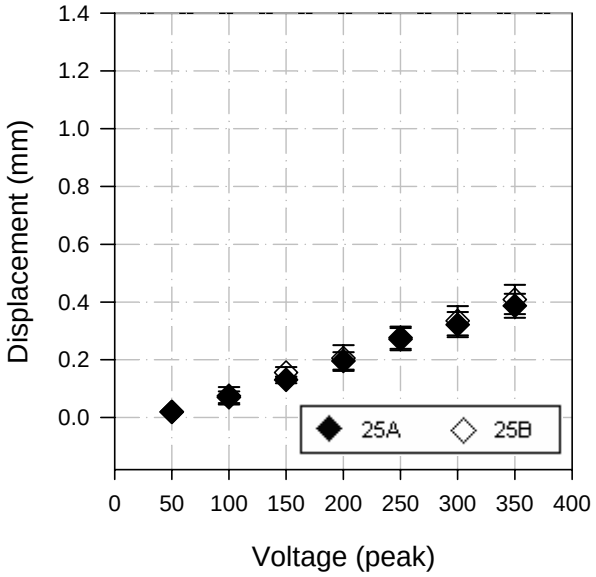

Figures 6.9. Average DC response of configurations 25A and 25B.

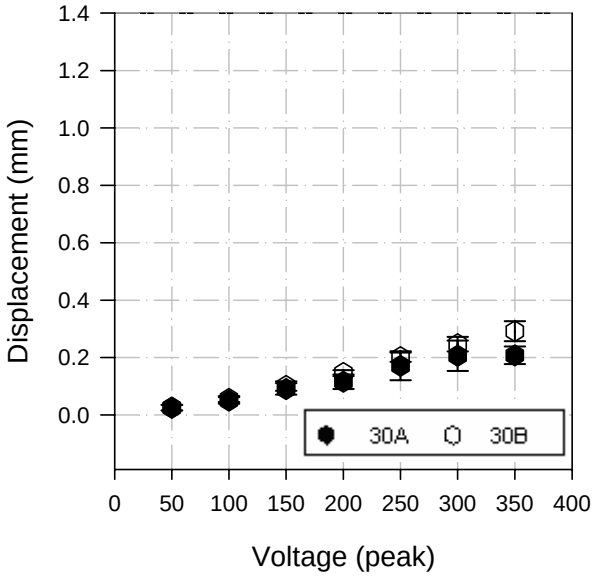

Figures 6.10. Average DC response of configurations 30A and 30B.

6.2 Displacement-Load Profiles

The displacement-load response of the devices was investigated using 0 to 1800 gram loads in tension. The response induced by mechanical loading provides researchers with a measure of the effective stiffness of the device. This data, in conjunction with other observed parameters, can be used to determine the amount of force the device can deliver as well as the work it is capable of expending for a given input. Graphs of the average center displacement developed in response to a given tensile load for prescribed device configurations are shown in Figures 6.11 -6.15.

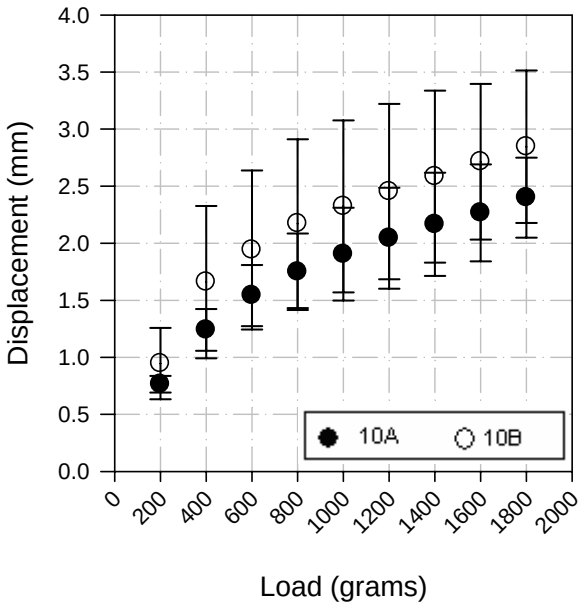

Figures 6.11. Average tensile response of configurations 10A and 10B.

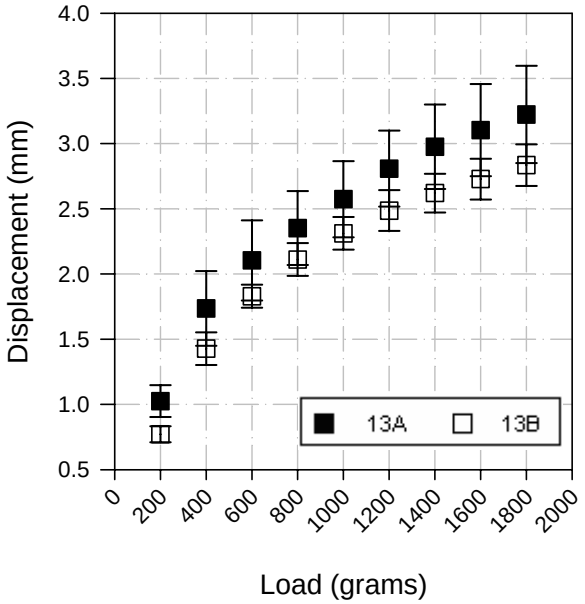

Figures 6.12. Average tensile response of configurations 13A and 13B.

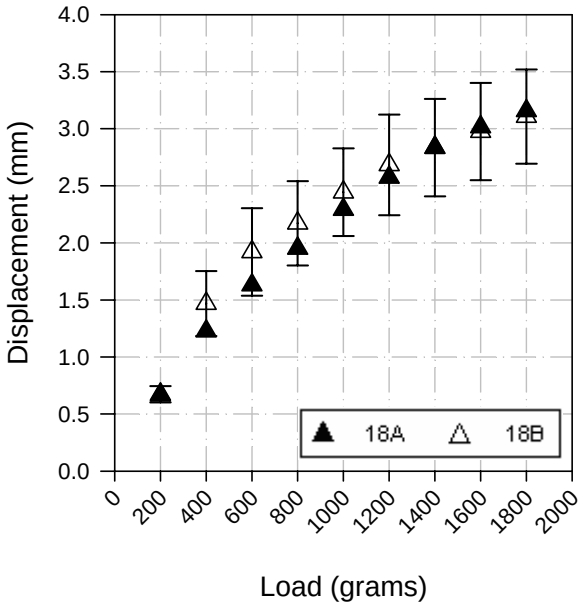

Figures 6.13. Average tensile response of configurations 18A and 18B.

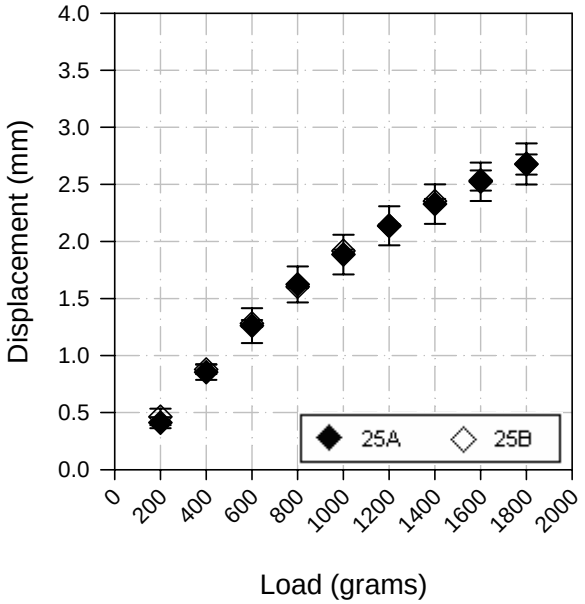

Figures 6.14. Average tensile response of configurations 25A and 25B.

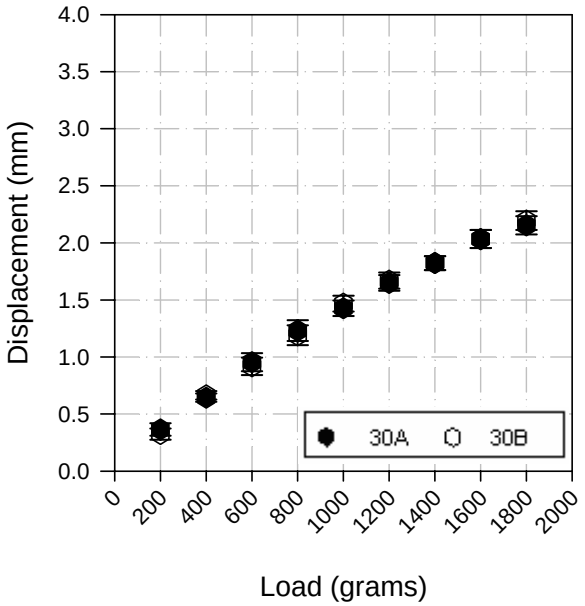

Figures 6.15. Average tensile response of configurations 30A and 30B.

Despite the differences observed in the magnitude of the displacements realized between similar devices constructed using thinner substrates and different adhesives, linear regressions of load-displacement data for devices constructed with similar substrates were found to have comparable slopes. That these slopes are within ten percent of each other suggests that the response of devices made with different adhesives is in fact quite similar. The baseline shift that is observed in the tensile-loaded displacement data, however, along with the differences seen between the step responses of A/B configurations, illustrates the importance of the mechanical properties of the adhesive and the role it plays in device performance. Table 6.2 shows the slopes found by fitting linear regressions to load-displacement data for the given device configurations. The table also presents the differences seen between slopes fit to data for similar devices that were constructed with different adhesives.

Table 6.2 Differences in slopes of tensile load induced displacement data for devices constructed with similar substrates and different adhesives

Configuration designation	Slope (mm/N)	Percent difference
10A	0.09	-9.54
10B	0.10	
13A	0.13	6.93
13B	0.12	
18A	0.16	10.72
18B	0.14	
25A	0.14	1.36
25B	0.14	
30A	0.11	-2.83
30B	0.12	

Differences in displacements seen between devices constructed with the same substrates and different adhesives were found to subside as substrate thickness increased.

The variation in the displacements measured for a given device configuration and tensile load were also found to be inversely related to substrate thickness, as shown by Figure 6.16. These trends suggest that the mechanical stiffness of the substrate plays an increasingly greater role in the response of the device as substrate thickness increases, as would be expected.

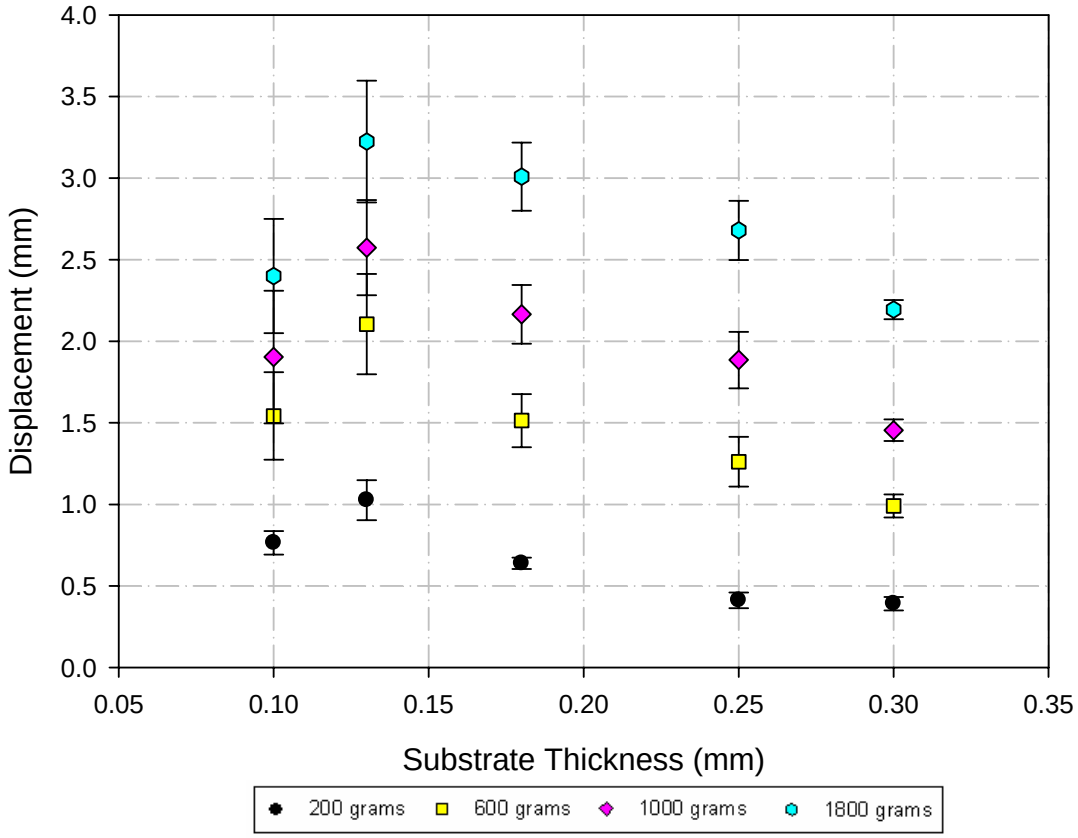

Figure 6.16 Tensile induced displacement as a function of substrate thickness for various loads.

6.3 Combined Loading Profiles

Investigating the displacement produced under combined loadings provides researchers with insight into the performance of the system under conditions similar to

those expected in practical application. Examining this response also allows researchers to investigate the coupling that exists between the electrical and mechanical properties of piezoelectric devices. Graphs of the average center displacement developed in response to combined tensile and AC voltage are shown in Figures 6.17 through 6.21. These graphs show the subsidence of apparent nonlinearities in the voltage-induced response as the magnitude of mechanical loading is increased. The linearity of response is also found to increase with substrate thickness, as illustrated by Figure 6.22. Results for the combined loading induced displacement for configurations not shown can be found in Appendix B.

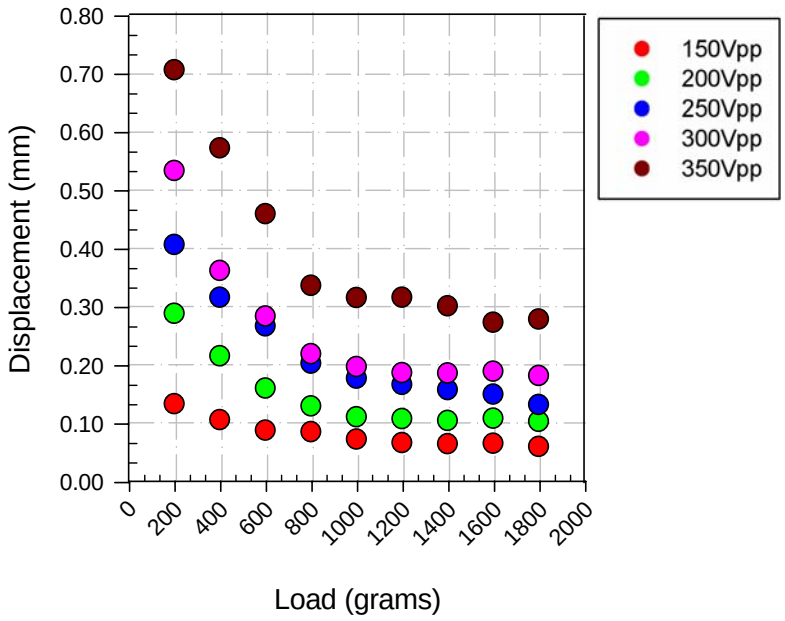

Figure 6.17. Average tensile and voltage induced response of configuration 10A.

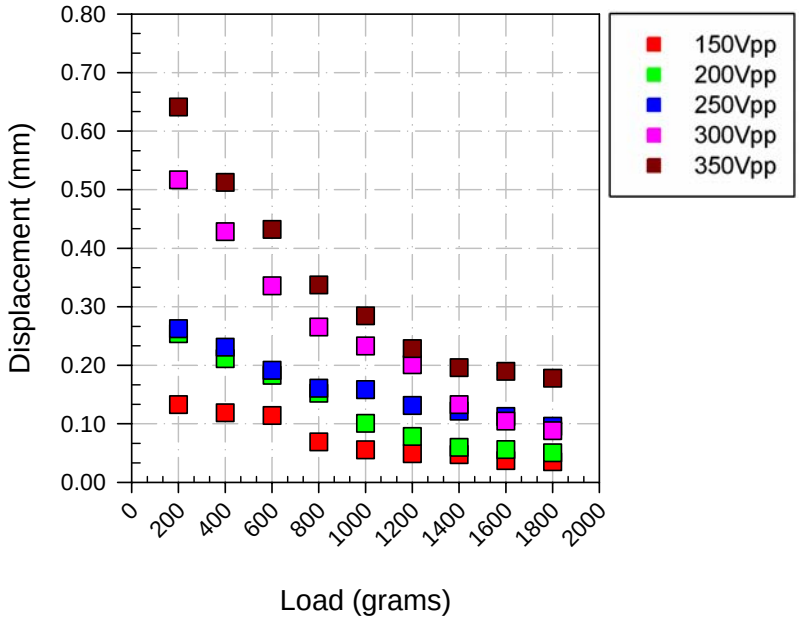

Figure 6.18. Average tensile and voltage induced displacement of configuration 13A.

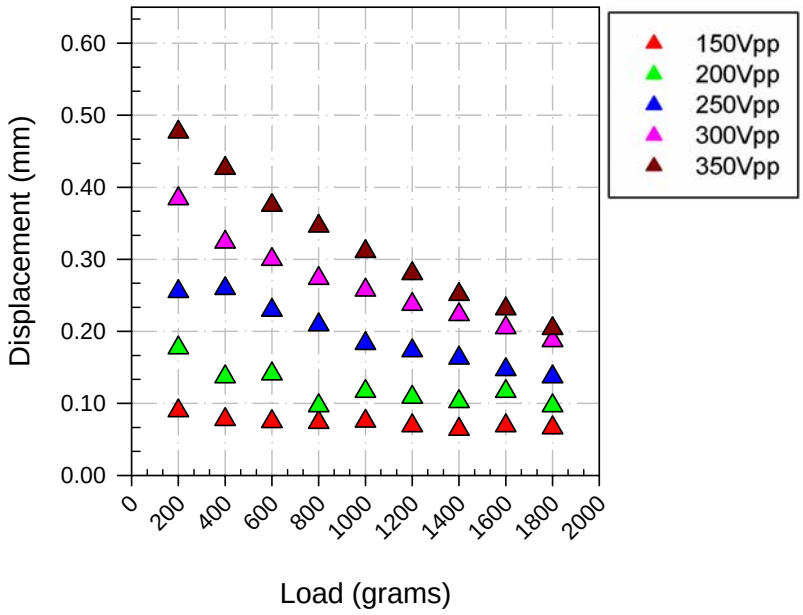

Figure 6.19. Average tensile and voltage induced displacement of configuration 18A.

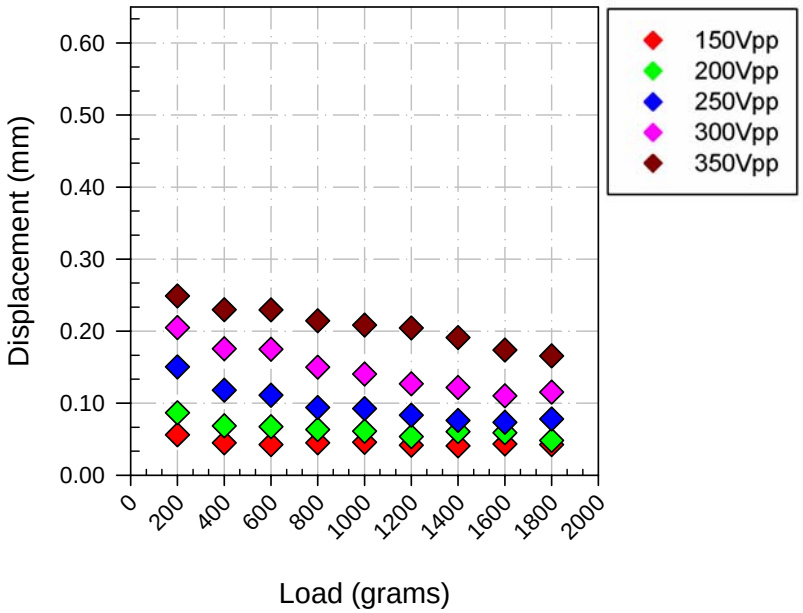

Figure 6.20. Average tensile and voltage induced displacement of configuration 25A.

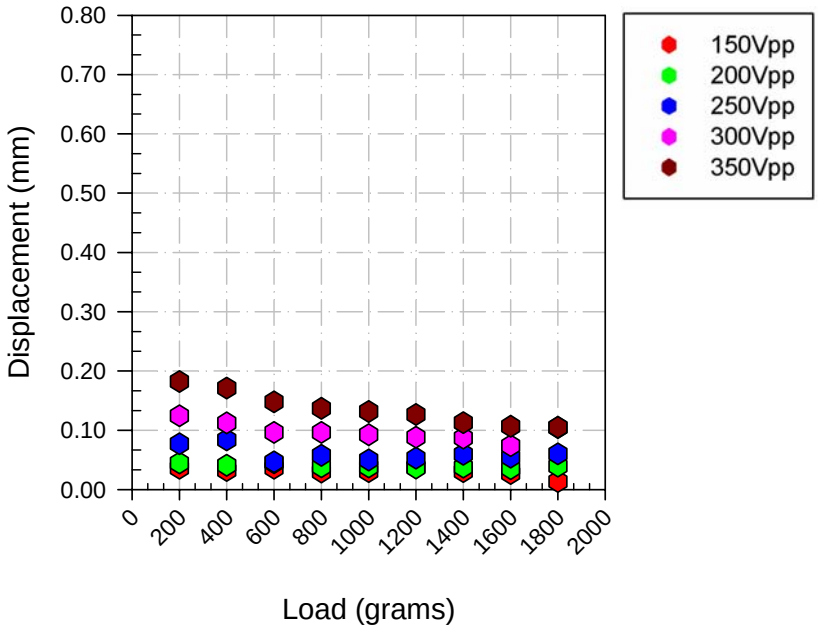

Figure 6.21. Average tensile and voltage induced displacement of configuration 30A.

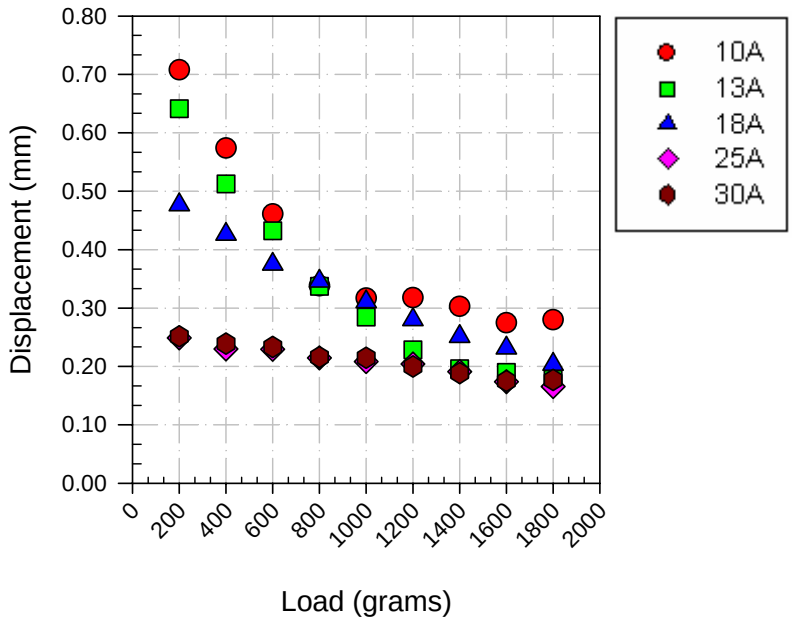

Figure 6.22 Average tensile and voltage induced displacement of various device configurations at 350Vpp.

6.4 Strain Profiles

Strain measurements were taken in response to DC and tensile mechanical loadings for prescribed device configurations. Tensile loading magnitudes between 0-1800grams were investigated, whereas, in the case of DC loading, voltages between 0 and 350Vp were used. Figures 6.23a-b show the tensile-induced strains developed in response to the fore mentioned range of mechanical loading. The graphs presented in Figure 6.23 show the opposing nature of longitudinal and transverse strains that are developed in response to mechanical loading.

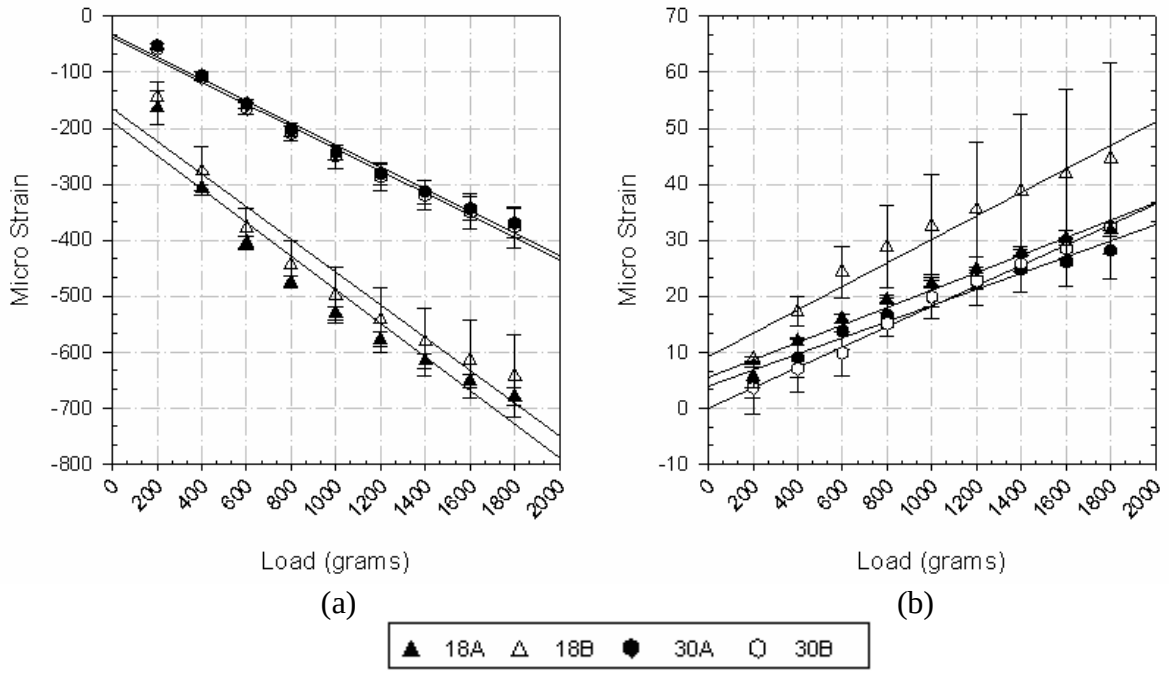

Figure 6.23 Tensile load induced strain in (a) the longitudinal and (b) the transverse directions.

The opposing nature of transverse and longitudinal mechanically-induced strains is not a phenomenon that is observed in voltage-induced loading scenarios. Under electrical loading, transverse and longitudinal strains have similar sign convention, and differences in the magnitude of strains developed are merely a factor of the geometry of the various layers [57]. This point is illustrated well in Figure 6.24a-b, as it shows that varying substrate thicknesses, and hence achieved displacements, have little effect on the magnitude of the strains developed in response to an electric field.

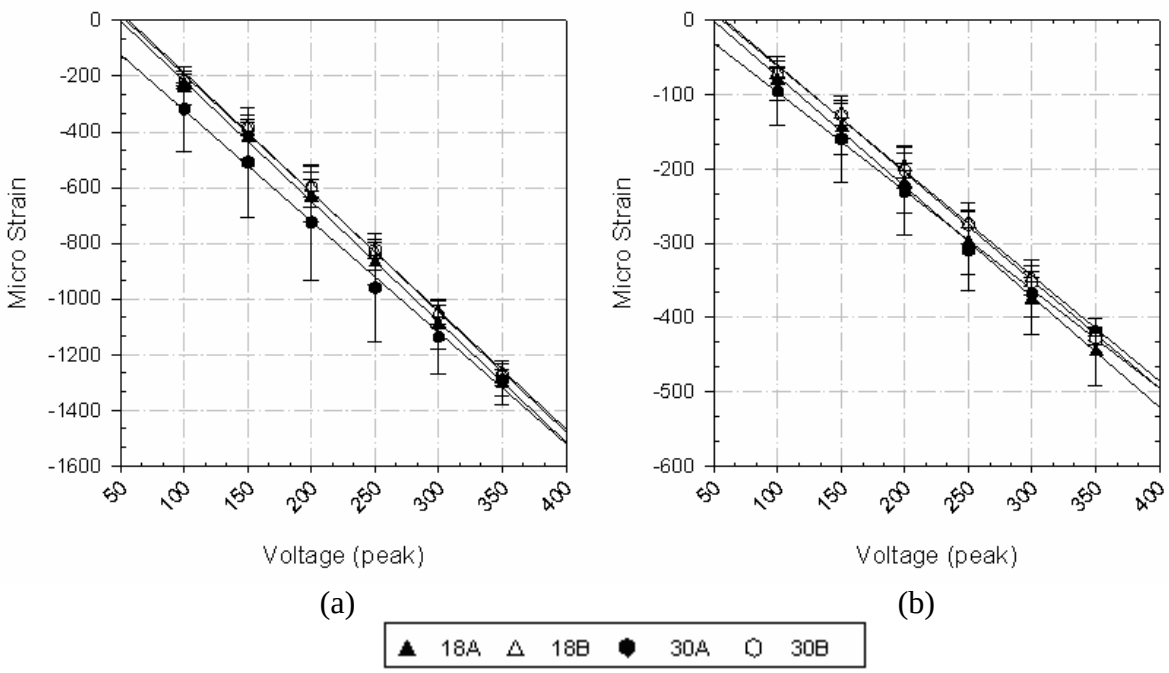

Figure 6.24 DC voltage induced strain in (a) the longitudinal and (b) the transverse directions.

6.5 Impedance Measurements

In order to efficiently design the circuitry to be used with devices like the MPC for actuation and energy harvesting applications, engineers require information concerning characteristics such as capacitance, natural frequency, and phase relations. With rudimentary models of piezoelectric behavior consisting primarily of resistive and capacitive elements, the electrical characteristics of piezo-based devices can be determined by investigating the frequency dependency of a device's impedance and capacitance. Reconnoitering such parameters can be effectively carried out by use of an impedance analyzer. In order to determine what effect, if any, the manufacturing process may have on the impedance characteristics of the ceramics used, the impedance and capacitance

characteristics of bare ceramics, as well as those incorporated in manufactured devices, were investigated. Figure 6.25a-b shows representative plots of the frequency dependence found in the impedance and capacitance of both bare piezoelectric plates and piezo elements incorporated in prestressed devices. Specifically, these plots show the typical impedance and capacitance, as a function of frequency, found in configuration 10B devices. It should be noted that when assessing these parameters for both bare ceramics and those incorporated in a post manufactured devices, measurements where taken at 1volt.

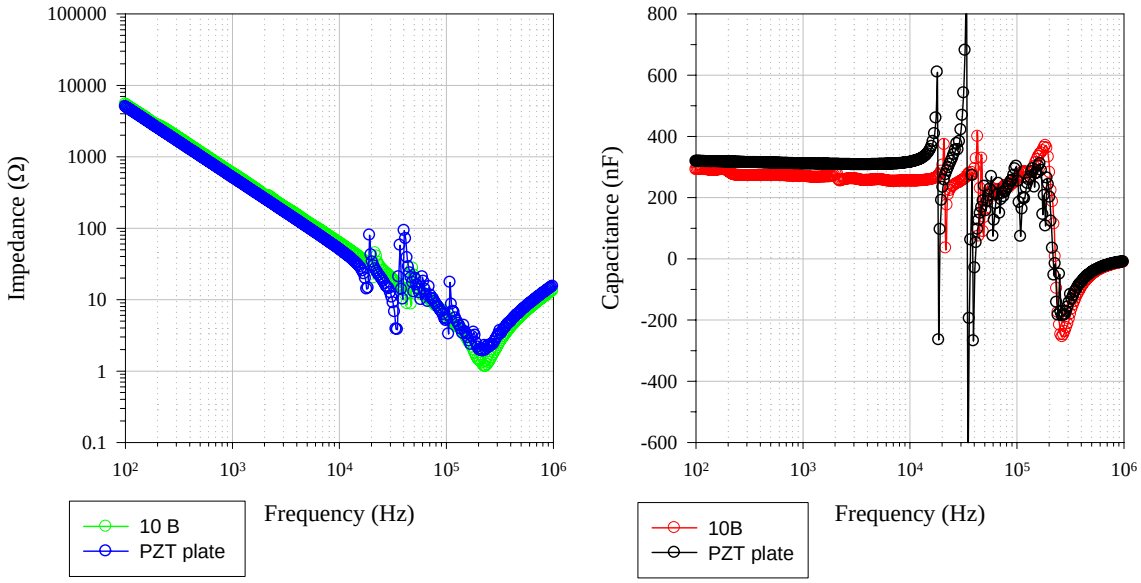

(a) (b)

Figure 6.25 Typical impedance and capacitance characteristics of PZT plates and configuration 10B devices as a function of frequency.

To allow for assessment of differences in the total impedance or capacitance of devices constructed with various substrates, the aforementioned electrical parameters were determined for each of the given device configurations. Results typical of a 10B configuration, and that of bare PZT plate, are presented in Figure 6.25a-b, while results

from the remaining investigations are presented in Appendix C. A comparison of the two results shown in Figure 6.25 reveals that consolidation of the piezoelectric element in the composite results in attenuation of the singularities found near electrical resonance. Despite this attenuation, the average value of the resistance and capacitance, for any given frequency, is not found to significantly vary from the values found for the bare ceramic plates. By examining the results shown in Appendix C, it can also be noted that the magnitude of the singularities observed near resonance are found to decrease with decreasing substrate thickness. This suggests that magnitudes of these singularities may be attributed to either the stiffness of the host structure or the magnitude of prestress placed on the piezoelectric element.

6.6 Summary Graphs

Two parameters that have been presented in the literature for purposes of facilitating the comparison of piezoelectric devices are the effective stiffness and the center displacement constant [4]. These parameters can be determined from the DC voltage induced, and tensile load induced, displacement responses of a device. The center displacement constant and effective stiffness are calculated by taking the inverse slope of an equation representing a linear fit to voltage or load induced displacement data, respectively. Figures 6.26 and 6.27 show the center displacement constant, and effective stiffness constant, as a function of substrate thickness, respectively.

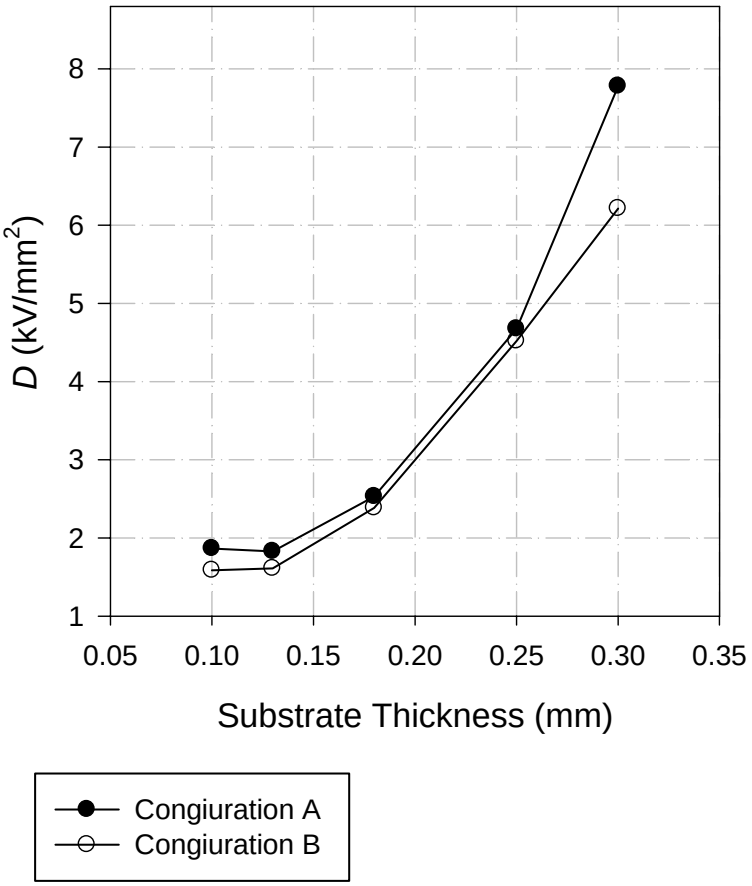

Figure 6.26 Center displacement constant as a function of substrate thickness

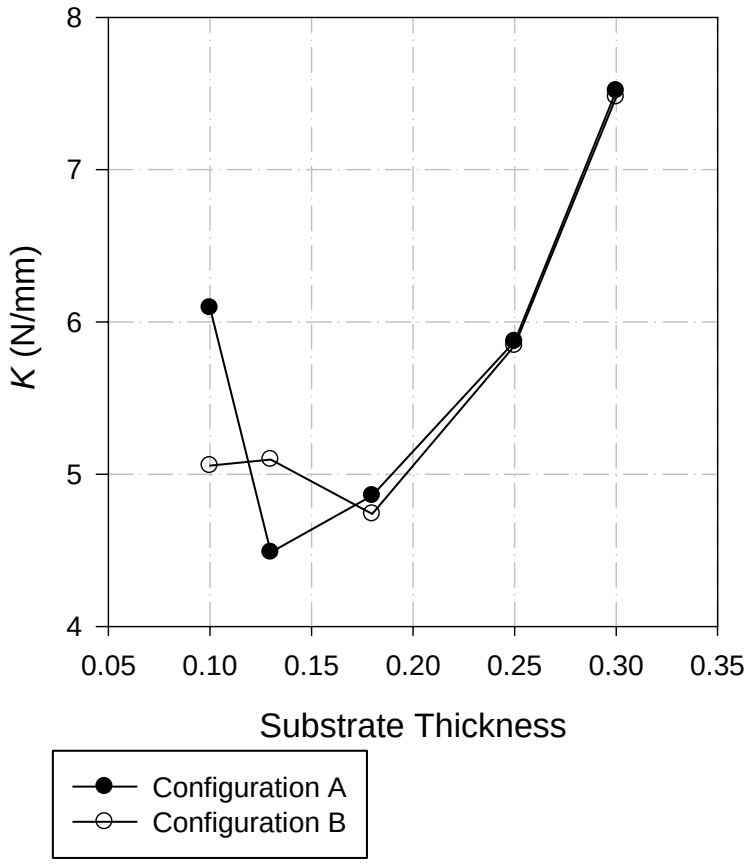

Figure 6.27 Effective stiffness as a function of substrate thickness

A linear fit of displacement data as a function of load, for a given voltage, provides designers with a means of predicting the magnitude of load which would effectively result in zero displacement. By deriving these equations, and defining a ninety percent reduction in displacement as an effective halt in displacement, the blocking force of the actuator at a given driving voltage can be determined. Figure 6.28 shows the blocking force for selected device configurations as a function of voltage. The parabolic relationship that the voltage verses blocking force data seems to allude to may be further evidence of the low-field and high-field electromechanical regimes that have been documented in the literature on

previous prestressed unimorphs [41]. Figure 6.29 shows the displacement–blocking force relationship displayed by selected device configurations at 350Vpp.

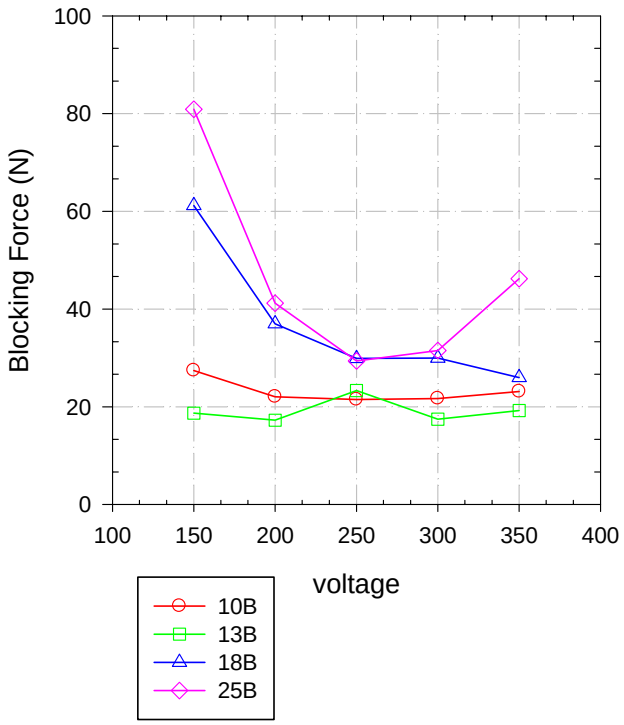

Figure 6.28 Blocking force as a function of voltage.

The data can be further investigated to determine a device's potential to do work under a given set of driving conditions. By multiplying the effective stiffness of the device by the inverse of the center displacement constant, a new parameter with units of work per given magnitude of driving field is defined. In the present investigation, this parameter was defined by units of Newton centimeters per kilovolt as shown by Equation 6.1. Normalizing the parameter with respect to the volume of the ceramic contained in the device allows for a relative assessment of efficiency with which the ceramic is utilized in the system.

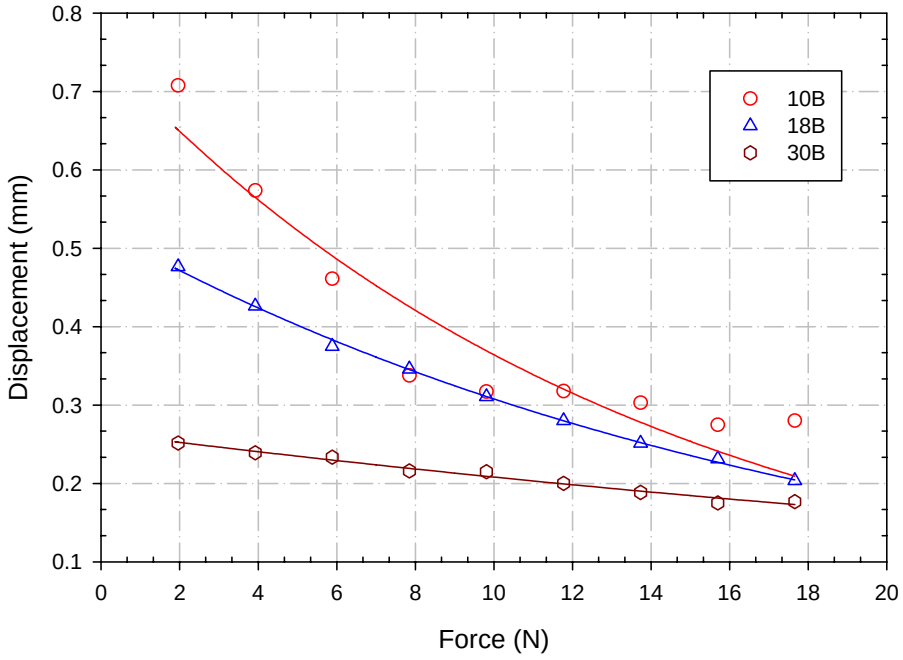

Figure 6.29 Blocking force as a function of displacement for configurations 10B, 18B, and 30B at 350Vpp.

Evaluating the newly presented parameter over the allowable voltage range of a device results in a measure of the work the device is theoretically displaying. Hence, the magnitude of this parameter is a measure of the mechanical work the device is capable of expending per given input. Table 6.3 shows the volume normalized magnitude of this parameter for the device configurations utilized in the present investigation.

$$K\left(\frac{N}{mm}\right)\cdot\frac{1}{D}\left(\frac{mm^2}{kV}\right)\cdot = u\left(\frac{N\cdot mm}{kV}\right) \qquad \text{Equation 6.1}$$

These figures suggest that devices constructed with adhesive B are capable of delivering more work for a given input voltage than devices constructed with adhesive A. Examining the potential work that is expected from the thermally prestressed unimorph Thunder® provides researchers with a means of comparing the two unimorph designs. The values calculated for the potential work of Thunder® devices that are shown in Table 6.4 were determined using magnitudes of the center displacement constant and effective stiffness found in the literature [4].

Table 6.3 Values of the MPC work constant for various configurations

	Potential Work /Ceramic Volume (N mm/kV)/mm^3	
Substrate Thickness (mm)	Adhesive A	Adhesive B
0.1	5.423E-03	5.296E-03
0.13	4.075E-03	5.257E-03
0.18	3.188E-03	3.301E-03
0.25	2.086E-03	2.147E-03
0.3	1.605E-03	1.998E-03

Table 6.4 Values of the Thunder® work constant for various configurations

Thunder® Configuration	Potential Work/ Ceramic Volume (N mm/kV)/mm^3
6R	9.236E-02
7Rx	1.621E-02
7R	1.685E-02
8R	4.150E-02

The magnitude of the values calculated for the normalized potential work of selected Thunder® devices was found to be an order of magnitude larger than that of MPC devices. These differences arises from the fact that, for the selected configurations, the effective stiffness for Thunder® devices were found to vary between 10 to 16.3 N/mm, while for MPC devices these values were found to be between 4.49 to 7.52 N/mm [4]. This gives an average value of effective stiffness for Thunder® devices of approximately 14 N/mm, and for MPC device 5.7 N/mm. With average values for the center displacement constants of the two devices being reasonably similar, the order-of-magnitude difference in average effective stiffness values can be identified as the source of the discrepancy between the achievable work found for the two sets of devices.

It is worth noting that the magnitudes of the potential work calculated using effective stiffness and center displacement constants can also be obtained, at specified voltages, from the information provided by the displacement-blocking force relations shown in Figure 6.29. To provide some transparency to the manner in which these two parameters relate, it is instructive to plot the magnitude of the parameters verse substrate thickness on a single graph, as shown in Figure 6.30. Keeping in mind that displacements

were found to decrease as substrate thickness increased, it is easy to see that configurations that produce the most displacement have the largest disparity between the values of these two parameters. Analyzing the results depicted in Figure 6.30 and Table 6.3 shows that as the magnitude of the center displacement constant converges with the magnitude of the effective stiffness, the amount of work the device is able to perform diminishes. That is to say, as the rigidity of the device increases, less displacement is achieved from a given electrical input, and hence the efficiency of the device is diminished.

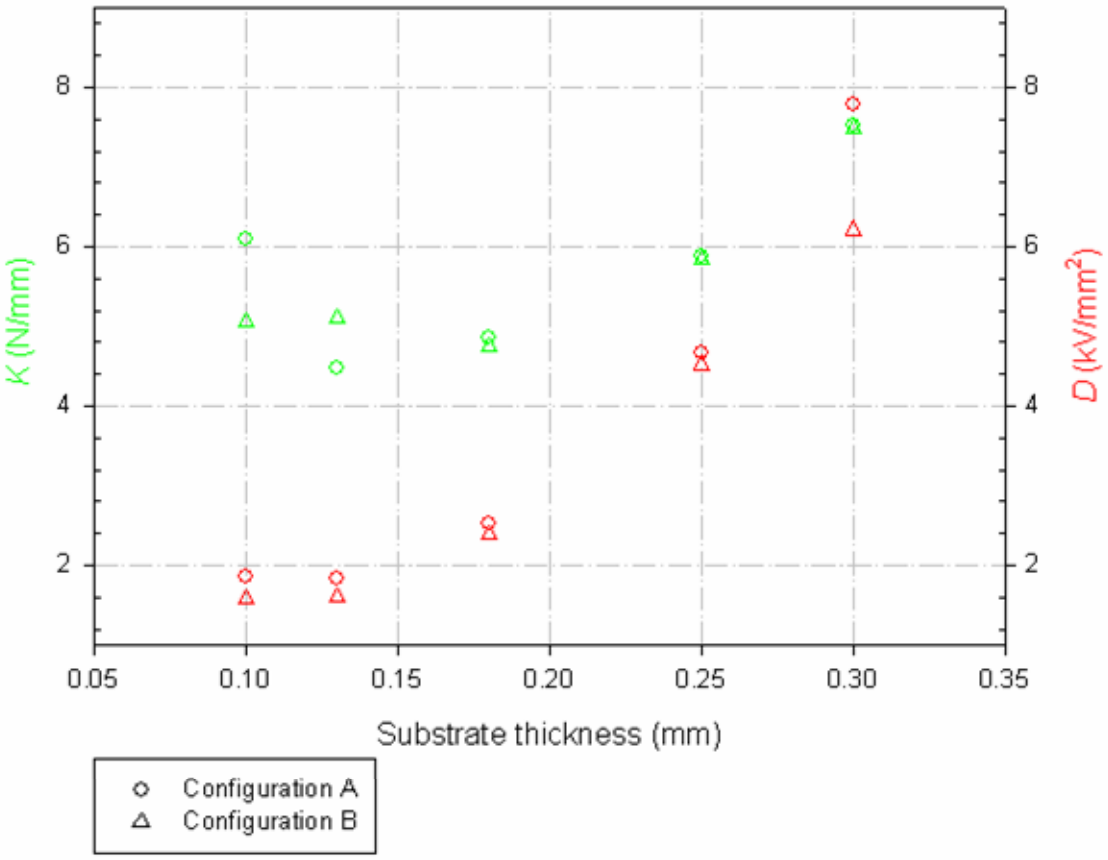

Figure 6.30 Relationship between the effective stiffness and center displacement constants as a function of substrate thickness

CHAPTER 7

CONCLUSIONS

The present investigation was undertaken to determine if a curved unimorph device could be constructed using mechanically-induced prestress as an alternative to the thermal prestressing currently utilized in the manufacturing of high performance unimorphs. In addition, factors that contributed to the enhanced performance of prestressed unimorphs were identified and modeled. Using information gained from the model, the form and layering sequence of the composite was defined along with manufacturing procedures for consolidating the constitutive materials. Results from a performance characterization of the resulting device were presented and compared with the performance characteristics of the commercially available Thunder® unimorphs. Although results show that a prestressed unimorph can be constructed using mechanical prestressing techniques, they also indicate that further investigation is needed to determine better suited joining mechanisms, if such device are to achieve the performance levels exhibited by thermally prestressed devices.

While thermally prestressed unimorphs are capable of achieving greater displacement and transmitting larger forces than traditional flat unimorphs, the processing methods used to construct these devices result in many undesirable effects. Thermally prestressed unimorphs have been investigated by a number of research groups whose findings indicate that the enhanced performance displayed by these devices is derived not only from the mechanical advantage gained from their curved form but also from the

extrinsic contributions to domain switching that is provided by the applied prestress [36]. In order to design a mechanically prestressed unimorph that possesses the same performance enhancing characteristics as thermally prestressed devices, researchers developed a unimorph design that utilizes a curved substrate to provide both mechanical advantage and prestress, which is known to enhance domain switching and hence overall piezoelectric efficiency. While increasing the curvature of the device contributes to both of the aforementioned performance enhancing characteristics, the maximum curvature of the device is limited by the ultimate tensile strength of the ceramic utilized in the composite. To determine the theoretical limits that are imposed on the maximum curvature of a device by this limiting factor, a model was developed which allowed researchers to define curvature induced stress in terms of material properties and thicknesses. Following the analytical formulation of the curvature limits, an experimental verification was undertaken to determine the relative accuracy of the model.

Experimental efforts were undertaken to determine the validity of the theoretically derived curvature limitations. Results from these efforts found a four percent difference between the theoretically and experimentally derived curvature limits. With analytical and empirical results in agreement, optimizing device performance through lamina sequence, and manufacturing procedures is now feasible. Detailed information concerning the finalized device form and manufacturing procedures can be found in Section 3.5 and Chapter 4, respectively.

In this work, composites were constructed using an elastic substrate that was plastically deformed to the desired radius of curvature. To consolidate the composite, a

pressure sensitive adhesive was utilized to bind the ceramic to the substrate as the curvature of the ceramic was slowly increased to match that of the substrate. The composite was then placed on a supporting structure and a pneumatic press was used to apply a uniform pressure of 175 kPa for a period of approximately 5 minutes to promote bonding. This method of consolidation proved effective, allowing for the construction of approximately 50 devices without resulting in ceramic fracture.

To determine the relative merit of the present class of prestressed unimorphs, a performance characterization of the device was undertaken. Traditional performance characteristics, such as center displacement constant and effective stiffness, were assessed, and a novel method for determining a devices capability to due work was introduced. To provide greater transparency when comparing devices of similar form and dissimilar dimension, the normalized potential work constant was introduced and defined as the amount of work a device is capable of producing with respect to the volume of piezoelectric material used in the device.

On average, the present class of devices was found to exhibit significantly larger tensile induced displacements than Thunder® devices. As a result, the average value of an effective stiffness constant for MPC device is smaller than that found for comparable Thunder® devices. The device configurations used in the present investigation resulted in effective stiffness constants of 4.49 to 7.52 N/mm. When comparing these values to the 10 to 16.3 N/mm found for similar sized Thunder® devices, it becomes apparent that MPC devices are in fact more compliant than Thunder® devices.

To provide a relative comparison of the DC induced displacements of MPC and Thunder® devices, attention was turned to the center displacement constant. Like the effective stiffness constant, the magnitude of this performance matrix is inversely correlated with the behavior it describes, i.e. displacement is the quotient obtained from dividing a given field by the center displacement constant. Hence, the larger the center displacement constant, the less displacement obtained from a given magnitude of field. For the MPC configurations investigated, the center displacement constant was found to vary between 1.59 to 7.78 kV/mm^2, while for Thunder® devices this parameter was found to vary between .71 to 3.85 kV/mm^2.

While values for the center displacement constants of both devices may appear to fall within a similar range it should be noted that the average value for MPC devices is more than double that found for Thunder® devices. Noting that the average effective stiffness of Thunder® devices is more than double that of MPC devices, it is easy to see that Thunder® devices are in fact more efficient actuators. However, a possible explanation for Thunder®'s superior performance can be obtained from examination of the step responses of the unimorphs shown in Appendix A. The DC induced displacement of Thunder® devices, like other piezo-based devices, exhibits creep in response to the constant driving field. In the case of the MPC devices, however, the step-induced displacement response shows an initial maximum displacement followed by an apparent relaxation that approaches a constant value. Not only does this trend provide a possible

explanation for the modest performance of the MPC devices, it may also be an indication of possible delamination.

Results indicate that mechanical prestressing is a viable alternative to the thermal prestressing methods currently utilized in the construction of high performance unimorphs. Performance evaluation of the present class of MPC devices indicate that mechanical prestressing is capable of producing a unimorph device that possesses the same performance enhancing characteristics found in thermally prestressed devices in spite of the indication of delamination caused by an adhesive. While further investigation is needed to develop a commercially viable mechanically prestressed composite design, the results presented indicate that the modeling and manufacturing techniques used in the present investigation can be used to aid development of future mechanically prestressed designs.

CHAPTER 8

FUTURE WORK

While the results presented in this work indicate that mechanical prestressing is a viable alternative to the thermal prestressing methods currently being utilized, additional research is needed before an assessment can be made regarding the commercial viability of mechanical prestressing techniques. Some of the issues that should receive further scrutiny before commercialization include: alternative joining mechanisms; more comprehensive modeling techniques; life cycle testing; and automated manufacturing capabilities. Further investigation into these issues will allow for increased efficiency, application specific optimization, determination of the average number of cycles before failure, and mass production.

To further develop MPC devices, assessing alternative joining mechanisms will be necessary. If MPC unimorphs are to obtain performance levels similar to those displayed by currently available devices, adhesives with greater rigidity must be implemented. Identifying more rigid joining mechanisms will allow for increased efficiency by decreasing mechanical dampening, thus enhancing achievable displacement and the overall stiffness of the device. Increasing the rigidity of the adhesive layer will allow for such enhancements by facilitate the transfer of energy from the ceramic to the underlying substrate resulting in greater efficiency. However, it will also facilitate the transfer of

energy from the substrate, and other layers of the device, to the ceramic, resulting in increased stress levels and the possibility of failure.

To help mitigate the increased probability of failure associated with more rigid joining mechanisms, comprehensive models of the composite should be developed that incorporate both electro-mechanical, and stress-strain behavior. Developing such models will allow designers to identify the geometric limitations imposed on device under operating conditions and predict its performance. These capabilities will allow designers to optimize the displacement and load handling abilities of a device by tailoring its geometric form and constitutive materials, based on the requirements of an application.

Following the development of more comprehensive mechanical models, an undertaking of life cycle testing should ensue. Establishing the relationship between prestress, effective stiffness, and the operational life of a device would benefit designers by allowing them to create devices with well rounded performance characteristics. To accurately determine the functionality of such relations, modeled results of the state of stress developed within the device should be used in conjunction with appropriate cycle failure analysis methods, and results should be compared with empirical data.

After researchers have conducted investigations into the issues outlined above, efforts should be directed toward producing automated manufacturing techniques and machinery. Such assets will undoubtedly prove vital in realizing the successful commercialization of MPC technology. To facilitate the success of commercialization efforts, manufacturing equipment should be designed such that it is capable producing a wide range of device configurations. By allowing the user to specify device parameters

such substrate material, thickness, and curvature, automated manufacturing equipment could be produced which would provide wide-ranging configuration variability.

While the research has shown that MPC technology is capable of producing high performance unimorph devices, additional work is needed before the technology is ready for commercial markets. To allow for successful commercialization, improved methods and materials for consolidating the composite need to be developed. Additionally, comprehensive mechanical models of the device and automated manufacturing capabilities need to be established. Until a thorough investigation of these issues has been undertaken, a definitive judgment on the relative merit of mechanical prestressing cannot be made.

Literature Cited

1. APC International, Ltd. www.americanpiezo.com

2. Face International www.faceinternational.com

3. Bryant, R.G., et al., *The Correlation of Electrical Properties of Prestressed Unimorphs as a Function of Mechanical Strain and Displacement.* Integrated Ferroelectrics, 2005. **71**: p. 267-287.

4. Dogan, A., K. Uchino, and R.E. Newnham, *Composite Piezoelectric Transducer with Truncated Conical Endcaps "Cymbal".* IEEE Transactions on Ultrasonics, Ferroelectrics, and Frequency Control, 1997. **44**(597-605).

5. Haertling, G.H., *RAINBOW ceramics- a new type of ultra-high displacement actuator.* American Ceramic Society Bull., 1994. **73**: p. 93-96.

6. Haris, A., et al., *Modeling and analysis for the development of Lightweight Piezoceramic Composite Actuators (LIPCA).* Computational Materials Science, 2004. **30**: p. 474-481.

7. Thomson, B.S., and Gandhi, M.V., *Smart Materials and Structures Technologies*. 1990, Lancaster: Technomic Publishing.

8. de Boer, E., *Theory of Motional Feedback.* IRE Transactions on Audio, 1961. **AU-9**: p. 15-21.

9. Janocha, H., *Actuators: Basics and Applications*. 1st ed. 2004, Saarbrucken: Springer. 336.

10. Herakovic, N., *Die Untersuchung der Nutzung des Piezoeffektor zur Ansteurung Fluide Ventille*. 1996, University of Aachen: Germany.

11. Park, G., et al., *Energy Harvesting for Structural Health Monitoring Sensor Networks.* 2007.

12. Granstorm, J., et al., *Energy harvesting from a backpack instrumented with piezoelectric shoulder straps.* Smart Materials and Structures, 2007. **16**: p. 1810-1820.

13. Anderson, E., N. Hagood, and J. Goodliffe, *Self-sensing piezoelectric actuation - Analysis and application to controlled structures*, in *NTRS*. 1992, NASA.

14. Jaffe, B., Cook, W., and Jaffe, H., *Piezoelectric Ceramics*. 1971, Marietta: R. A. N. Publishers. 317.

15. Boyd, J.G., *Thermomechancial response of shape memory composites.* Intelligent Materials and Structures, 1993. **5**: p. 333-346.

16. Shu, S., et al., *Modeling of a flexible beam actuated by shape memory alloy wires.* Smart Materials and Structures, 1997. **6**: p. 265-277.

17. U.S.F.D.A, *New Device Approval*, in *CDRH Consumer Information*. 2003.

18. Murphy, T.P., *Comparing the SMART Stent with the Wallstent Iliac Endoprosthesis: Reading Between the Lines.* Journal of Vascular and Interventional Radiology, 2004. **15**: p. 907-909.

19. Winslow, W., *Method and means for translating electrical impulses into mechanical force*. 1947: US.

20. Winslow, W., *Induced fibration of suspensions.* Applied Physics, 1949. **20**: p. 1137-1140.

21. Suplee, C., *Is the Sky the Limit in the Future?*, in *Virginian-Pilot*. 1997. p. D4.

22. Curie, P. and J. Curie, *Development by pressure of polar electricity in hemihedral crystals with inclined faces.* Bull. soc. min. de France, 1880. **3**: p. 90-93.

23. Ballato, A., *Piezoelectricity: History and New Thrusts.* IEEE Ultrasonics Symposium, 1996: p. 575-583.

24. Boston Piezo-Optics Inc. www.bostonpiezooptics.com

25. Sawyer, C.B., *The Use of Rochelle Salt Crystals for Electrical Reproduces and Microphones.* Proceedings of the Institute of Radio Engineers, 1931. **19**: p. 2020-2029.

26. Dogan, A., J. Tressler, and R.E. Newnham, *Solid-State Ceramic Actuator Designs.* AIAA, 2001. **39**(7).

27. Niezrecki, C., et al., *Piezoelectric Actuation: State of the Art.* The Shock and Vibration Digest, 2001. **33**(4): p. 269-280.

28. Ramsay, J.V. and E.G.V. Mugridge, *Barium Titanate Ceramics for Fine-Movement Control.* Journal of Scientific Instruments, 1962. **39**: p. 636-637.

29. Newnham, R.E., et al., *Flextensional "Moonie" Actuators.* IEEE Ultrasonics Symposium, 1993: p. 509-513.

30. Xu, Q.C., et al., *Ceramic-metal Composite Actuator.* IEEE Ultrasonics Symposium, 1991(923-928).

31. Sugawara, Y., et al., *Metal-Ceramic Composite Actuators.* Journal of the American Ceramic Society, 1992. **75**: p. 996-998.

32. Mossi, K., *Thin-Layer Pre-Stressed Composite Ferroelectric Driver and Sensor Characterization with application to Separation Flow Control*, in *Mechanical Engineering*. 1998, Old Dominion University: Norfolk. p. 186.

33. Smith, B., N.S. Goo, and K. Mossi. *Experimental Development of Power Consumption in LIPCA-C2*. in *Behavior and Mechanics of Multifunctional and Composite Materials*. 2007. San Diego: SPIE.

34. Schwartz, R.W., et al. *Understanding Mechanics and Stress Effects in Rainbow and Thunder Stress-biased Actuators*. in *Smart Structures and Materials 2000: Active Materials: Behavior and Mechanics*. 2000: SPIE.

35. Schwartz, R.W. and M. Narayanan, *Development of High performance stress-biased actuators through the incorporation of mechanical pre-loads.* Sensors and Actuators, 2002. **101**: p. 322-331.

36. Schwartz, R.W. and Y.W. Moon, *Domain Configuration and Switching Contributions to the Enhanced Performance of Rainbow Actuators.* SPIE Smart Structures and Materials, Active materials: Behavior and Mechanics, 2001. **4333**(408).

37. Hyer, M.W. and A.B. Jilani, *Deformation characteristics of circular RAINBOW actuators.* Smart Materials and Structures, 2002. **11**: p. 175-195.

38. Bryant, R.G., *LaRC-SI: A Soluble Aromatic Polyimide.* High Performance Polymers, 1996. **8**: p. 607-615.

39. Fox, R., Hellbaum, R., Bryant, R., and Copeland, B., *Advanced Layered composite polylaminate electroactive actuator and sensor*. 1997: US.

40. Usher, T. and A. Sim, *Nonlinear dynamics of piezoelectric high displacement actuators in cantilever mode.* Journal of Applied Physics, 2005. **98**.

41. Ounaies, Z., et al. *Low-field and high-field characterization of THUNDER actuators*. in *Smart Structures and Materials 2001: Active Materials: Behavior and Mechanics*. 2001: SPIE.

42. Pinkerton, J.L. and R.W. Moses, *A Feasibility Study To Control Airfoil Shape Using THUNDER*, in *NASA Technical Memorandum 4767*. 1997.

43. Kymissis, J., et al. *Parasitic Power Harvesting in Shoes*. in *Second IEEE International Conference on Wearable Computing*. 1998.

44. Mossi, K., Z. Ounaies, and S. Oakley. *Optimizing Energy Harvesting of a Composite Unimorph Pre-Stressed Bender*. in *Proceedings of The American Society For Composites*. 2001. Virginia Tech Blacksburg, Virginia.

45. Green, C., *Low Frequency Energy Harvesting Using Clamped Pre-Stressed Unimorphs Diaphragms*, in *Mechanical Engineering*. 2006, Virginia Commonwealth University: Richmond. p. 121.

46. Niezrecki, C. and S. Balakrishnan. *Power Characterization of THUNDER Actuators as Underwater Propulsors*. in *Smart Structures and Materials 2001: Smart Structures and Integrated Systems*. 2001: SPIE.

47. Goldfrab, M., et al. *Elastodynamic Locomotion in Mesoscale Robotic Insects*. in *Smart Structures and Materials 1999: Electroactive Polymer Actuators and Devices*. 1999.

48. Cattafesta, L., et al., *Review of Active Control of Flow-Induced Cavity Resonance.* AIAA, 2003. **33**: p. 3567.

49. Mane, P., *Experimental design and Analysis of Piezoelectric Synthetic Jets in Quiescent Air*, in *Mechanical Engineering*. 2005, Virginia Commonwealth University: Richmond. p. 116.

50. Niezrecki, C. and H.H. Cudney. *Feasibility of Using Piezoelectric Actuators to Control Launch Vehicle Acoustics and Structural Vibrations*. in *Proceedings of the SPIE 7th International Symposium on Smart Structures and Materials*. 2000. Newport Beach, California.

51. Corsaro, R.D. *Lightweight Low Frequency Woofer for Active Sound Control in Payload Fairings*. in *Smart Structures and Materials 2001: Industrial and Commercial Applications of Smart Structures Technologies*. 2001.

52. Aimmanee, S. and M.W. Hyer, *Analysis of the manufactured shape of rectangular THUNDER-type actuators.* Smart Materials and Structures, 2004. **13**(6): p. 1389-1406.

53. Webber, K.G., D.P. Hopkinson, and C.S. Lynch, *Application of a Classical Lamination Theory Model to the Design of Piezoelectric Composite Unimorph Actuators.* Journal of Intelligent Material Systems and Structures, 2006. **17**(1): p. 29-34.

54. Mossi, K., et al., *Shape modeling and validation of stressed biased piezoelectric actuators.* Smart Materials and Structures, 2006. **15**(1785-1793).

55. Mossi, K., R. Bryant, and P. Mane, *Piezoelectric Composite as Bender Actuators.* Integrated Ferroelectrics, 2005. **71**: p. 221-232.

56. Balakrishnan, S. and C. Nierecki, *Investigation of Thunder Actuators as Underwater Propulsors.* Journal of Intelligent Material Systems and Structures, 2002. **13**(4): p. 193-207.

57. Aimmanee, S., *Deformation and Force Characteristics of Laminated Piezoelectric Actuators*, in *Engineering Mechanics*. 2004, Virginia Tech: Blacksburg, Virginia. p. 280.

58. Cappelleri, D.J., M.I. Frecker, and T.W. Simpson. *Optimal Design of A PZT Bimorph Actuator for Minimally Invasive Surgery*. in *7th International Symposium on Smart Structures and Materials*. 1999. Newport Beach, CA: SPIE.

59. Haertling, G.H., *Method for making monolithic prestressed ceramic devices*. 1995: US.

60. Ochinero, T.T. and M.W. Hyer, *Manufacturing Distortions of Curved Composite Panels.* Journal of Thermoplastic Composite Materials, 2002. **15**: p. 79-87.

61. Hibbeler, R.C., *Mechanics of Materials*. fifth ed. 2003, Upper Saddle River, New Jersey: Pearson Education , Inc.

62. Guillon, O., F. Thiebaud, and D. Perreux, *Tensile fracture of soft and hard PZT.* International Journal of Fracture, 2002. **117**: p. 235-246.

63. CTS Corporation http://www.ctscorp.com/default.htm

APPENDIX A

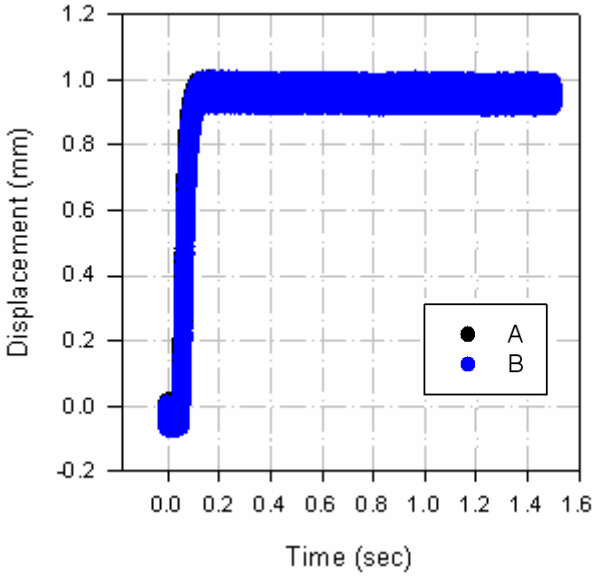

Typical step response of 10A and 10B configurations

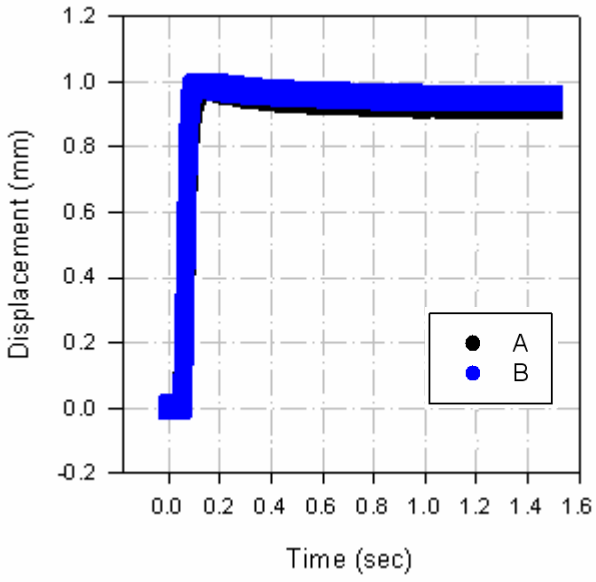

Typical step response of 13A and 13B configurations

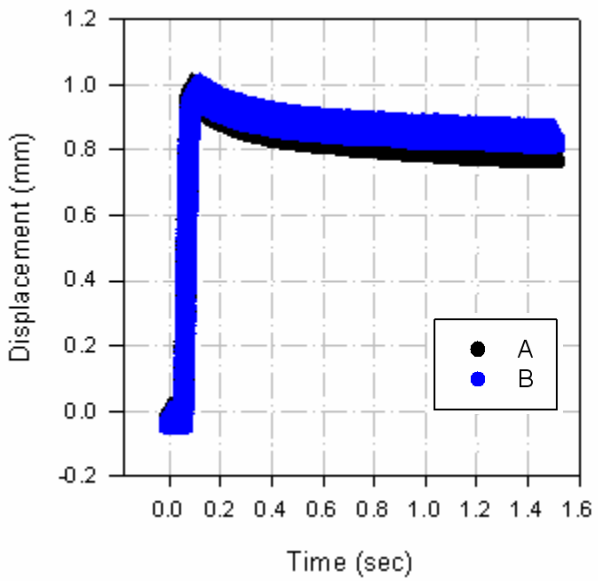

Typical step response of 18A and 18B configurations

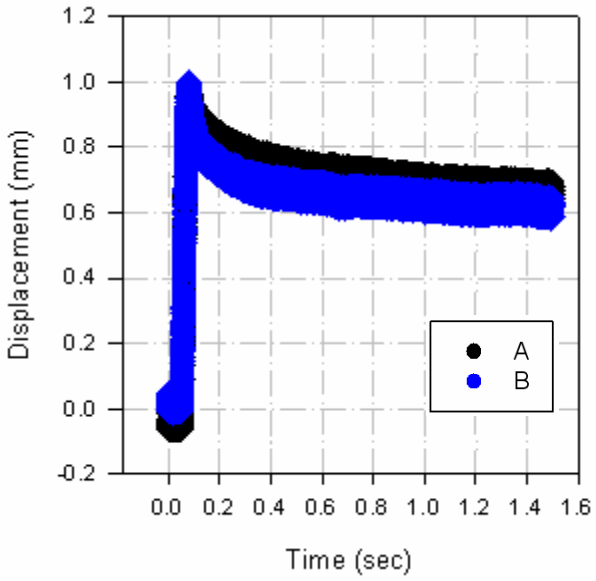

Typical step response of 25A and 25B configuration

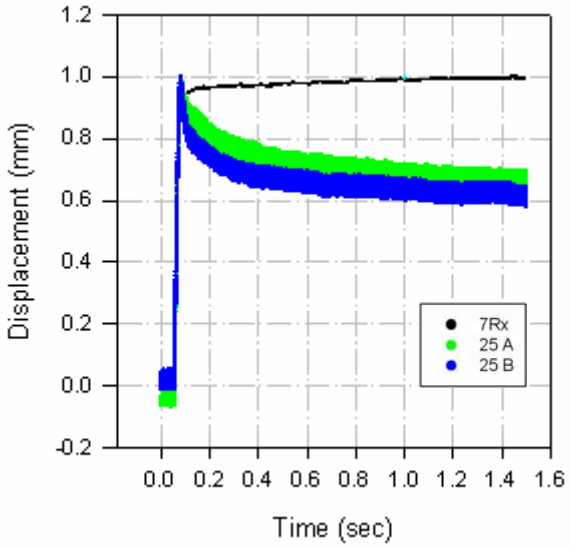

Step response of Thunder® 7Rx, and MPC 25A and 25B

APPENDIX B

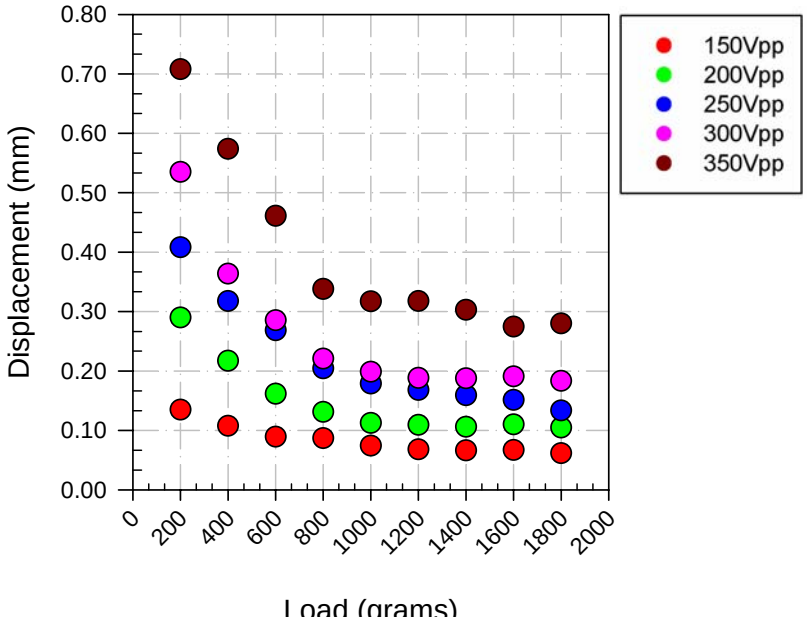

Averaged tensile and voltage induced response of configuration 10B.

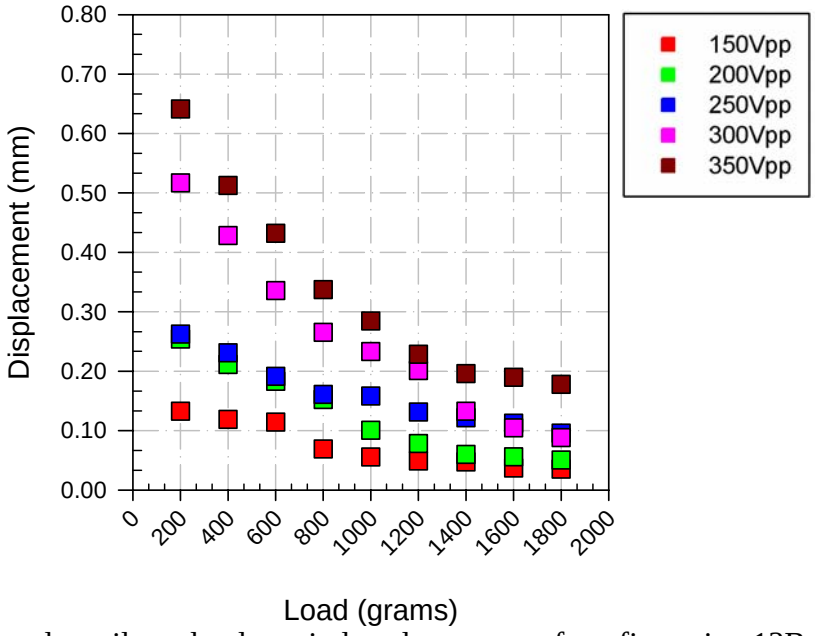

Averaged tensile and voltage induced response of configuration 13B.

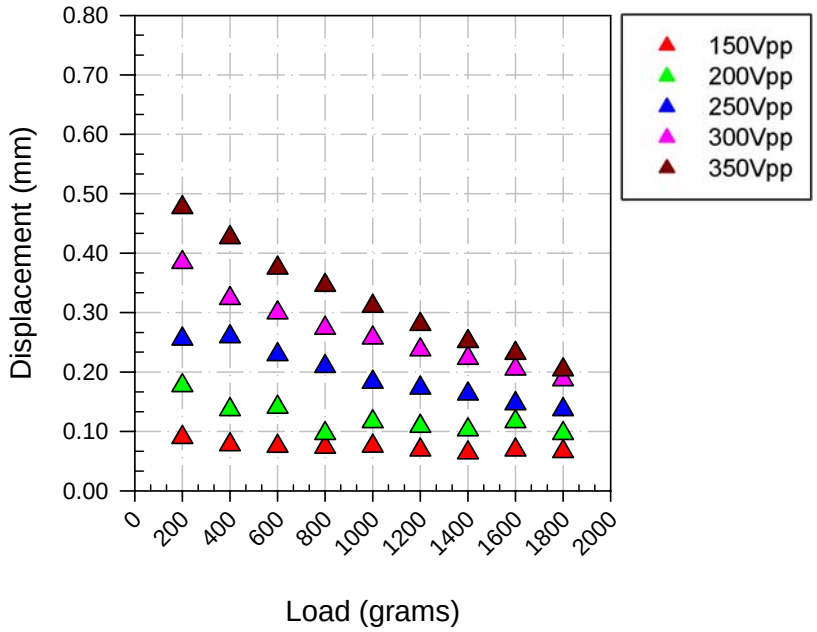

Averaged tensile and voltage induced response of configuration 18B.

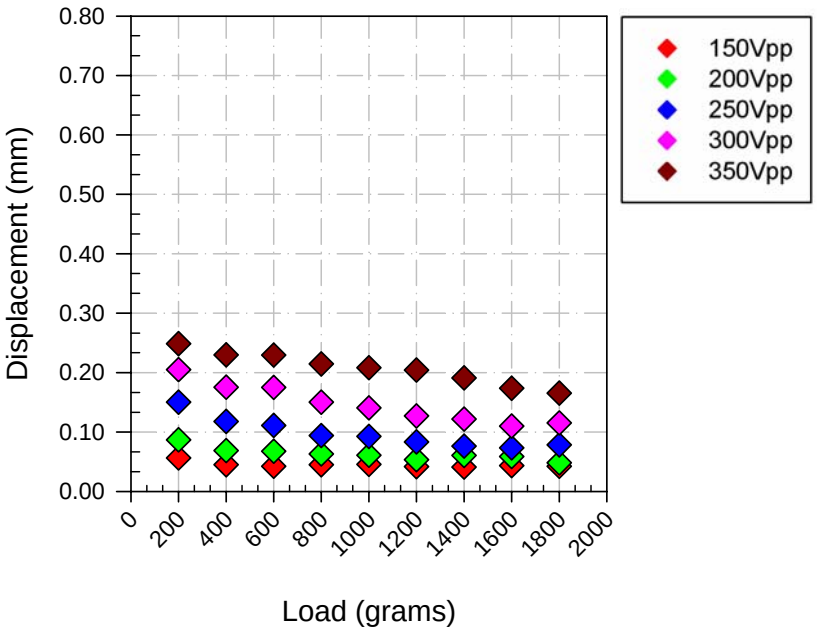

Averaged tensile and voltage induced response of configuration 25B.

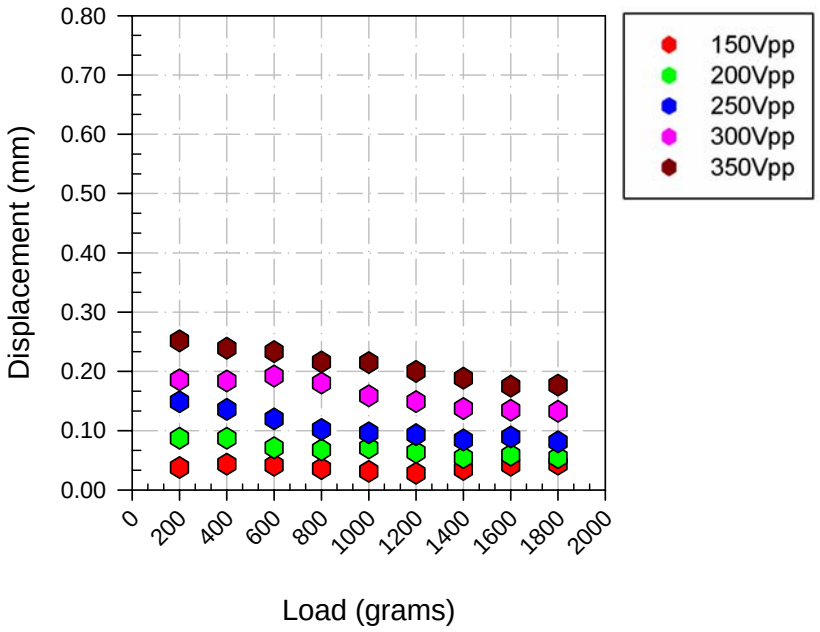

Averaged tensile and voltage induced response of configuration 30B.

APPENDIX C

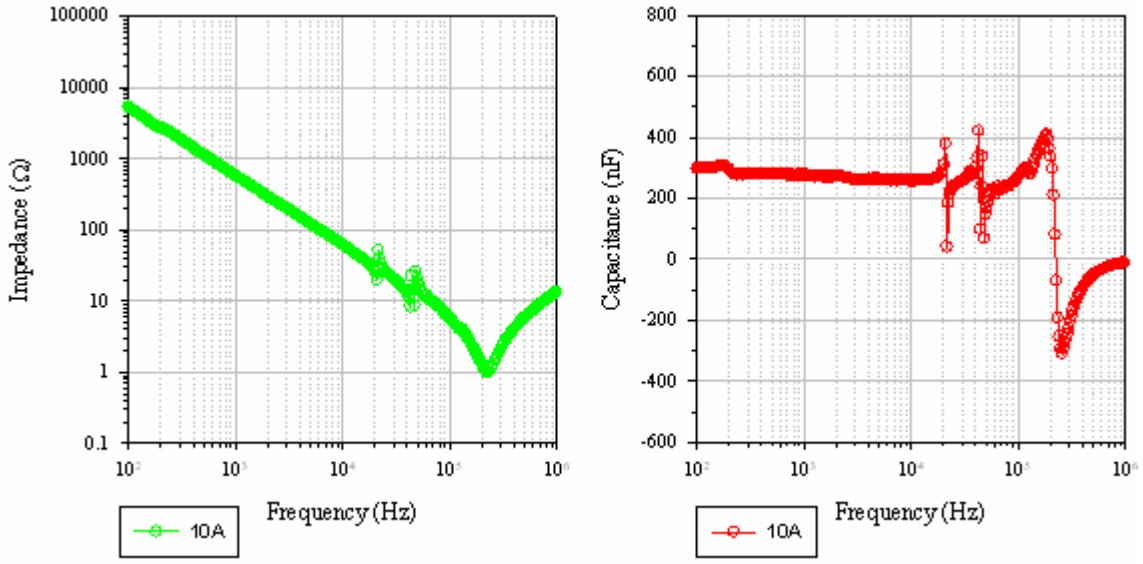

Typical impedance and capacitance characteristics of an MPC configuration 10A as a function of frequency.

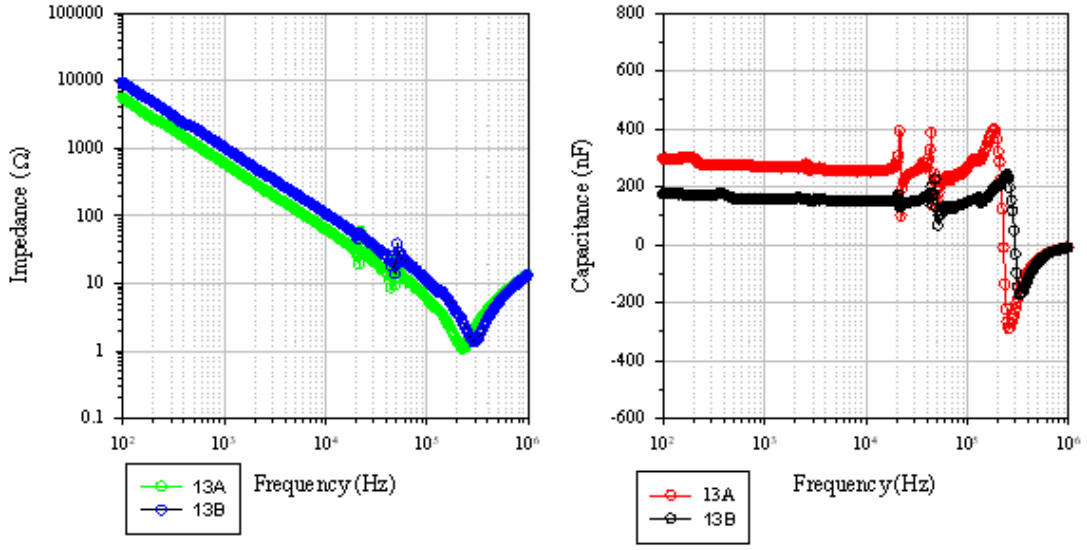

Typical impedance and capacitance characteristics of an MPC configuration 13A and 13B as a function of frequency.

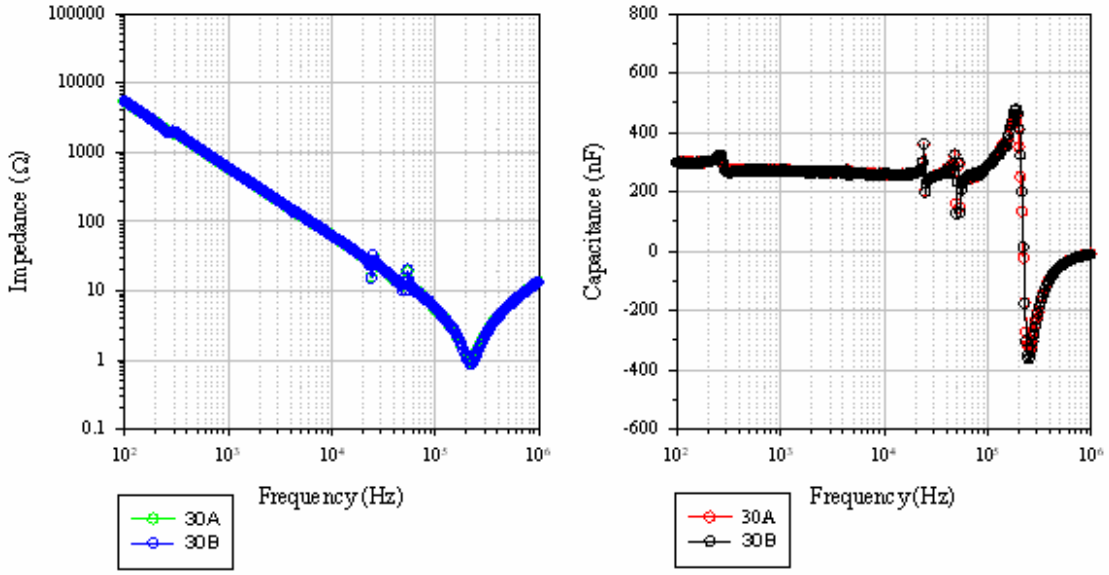

Typical impedance and capacitance characteristics of an MPC configuration 30A and 30B as a function of frequency.

APPENDIX D

FASTEN. BOND. SEAL.

Avery Dennison™ MS 3032 SL Spec # 56520

Transfer Tape

AVERY DENNISON

Specialty Tape Division

250 Chester Street
Painesville, Ohio 44077
Phone: 866-GO-AVERY (866-462-8379)
Fax: 440-398-3298
email: psa.tape@averydennison.com
URL: stus.averydennison.com

Surface Preparation
It is essential, as with all pressure-sensitive tapes, that the surface to which the tape is applied be clean, dry, and free of grease or oil.

US Patent No. 4812541

Temperatures

Min Application Temp	50° F	10° C
Max Continuous Operating Temp	300° F	149° C
Max Intermittent Operating Temp	400° F	204° C

Storage and Shelf Life
One year when stored at 70ºF (21ºC) 50% RH out of direct sunlight.

Underwriters Laboratories Inc. Surface Burning Characteristics to
UL 969 Flame Spread - Smoke Developed -

Limited Warranty

All statements, technical information and recommendations concerning products sold or samples provided by AVERY DENNISON are based upon tests believed to be reliable but do not constitute a guarantee or warranty. All products are sold and samples of products provided with the understanding that PURCHASER has independently determined the suitability of such products for its purposes. AVERY DENNISON warrants the products to be free from defects in material and workmanship. Should any failure to conform to this warranty appear within one year after the initial date of shipment, AVERY DENNISON shall, upon notification thereof and substantiation that the products have been stored and applied in accordance with AVERY DENNISON's standards, correct such defects by suitable repair or replacement without charge at AVERY DENNISON's plant or at the location of the products (at AVERY DENNISON's election) provided, however, if AVERY DENNISON determines that the repair or replacement is not commercially practical, AVERY DENNISON shall issue credit in favor of PURCHASER in an amount not to exceed the purchase price of the products.

This warranty is exclusive and is in lieu of any implied warranty of merchantability, fitness for a particular purpose or other warranty of quality, whether express or implied, except the warranty of title and against patent infringement. No waiver, alteration, additions or modifications of the foregoing conditions shall be valid unless made in writing and manually signed by an officer of Avery Dennison. "Or in the time period stated on the specific product specification sheet, if any, and if not then on the specific product information literature in effect at time of shipment.

Limitation of Liability

In no event shall AVERY DENNISON be liable for any incidental or consequential damages, including but not limited to, loss of profit, loss of use of production or loss of capital. The remedies of PURCHASER set forth herein are exclusive and the total liability of AVERY DENNISON with respect to any contract, or anything done in connection therewith such as the performance or breach hereof, or from the manufacture, sale, delivery, resale, installation or use of products whether arising out of contract, negligence, strict tort, or under any warranty, or otherwise, shall not exceed the purchase price of the products upon which the liability is based.

PRODUCT DESCRIPTION

Applications
Specially designed for use on membrane touch switch assemblies and graphic overlays

Features
Unsupported specially formulated acrylic adhesive
Adhesive protected by moisture stable polycoated liners
Good adhesion to high surface energy plastics and metals

Benefits
Excellent shear strength
Chemical and UV resistance
Ease of die-cutting and liner removal
Moisture stable liner provides layflat for easy processing

PRODUCT DATA

(Not for Specification Use)

Product Construction Test Methods: PSTC-33, ASTM D-1000, TAPPI T-411-M-44

		US Mils	MM's
Adhesive	Acrylic	2.0	0.05
Liner	58 # Natural Poly-coated Kraft	4.3	0.11
	Total Construction	6.3	0.16

Adhesive Properties

Peel Adhesion Test Method(s): PSTC-3, ASTM D-3330, STD-10
2 mil PET 180° 12" min Initial

Substrate	Test Side	Lbf / in	US Oz / in	N / Meter
SS	Liner	5.3	85	928

Peel Adhesion Test Method(s): PSTC-3, ASTM D-3330, STD-10
2 mil PET 180° 12" min Initial

Substrate	Test Side	Lbf / in	US Oz / in	N / Meter
PP	Liner	4.0	64	700

Peel Adhesion Test Method(s): PSTC-3, ASTM D-3330, STD-10
2 mil PET 180° 12" min Initial

Substrate	Test Side	Lbf / in	US Oz / in	N / Meter
PET	Liner	5.4	86	946

Peel Adhesion Test Method(s): PSTC-3, ASTM D-3330, STD-10
2 mil PET 180° 12" min Initial

Substrate	Test Side	Lbf / in	US Oz / in	N / Meter
Polycarbonate	Liner	7.6	122	1331

Static Shear Test Method(s): PSTC-7, ASTM D 3654, STD-9
2 mil PET @ 72°F / 22°C 1/2" sq (3.25 cm2) 500 g

Substrate	Test Side	Min to Fail
SS	Liner	> 10,000

Static Shear Test Method(s): PSTC-7, ASTM D 3654, STD-9
2 mil PET @ 72°F / 22°C 1/2" sq (3.25 cm2) 1000 g

Substrate	Test Side	Min to Fail
SS	Liner	> 10,000

Avery Dennison™ FT 2002

Physical Properties	Typical Values		Units	Test Methods
THICKNESS				
Adhesive	50		microns	ATM .7
Liner :	128		microns	
Total	178		microns	
TACK (Finat)	630		N/m	ATM.8-FINAT.9
ADHESION (180°peel)	20min	24h	N/m	ATM.1-PSTC.1
Stainless steel	460	590		
Polycarbonate	420	480		
Polyester	420	440		
Rigid polypropylene	200	220		
SHEAR RESISTANCE	(Static)		min.	ATM.2-FINAT.8-
25x25mm –1 kg	> 10.000			PSTC.7
TEMPERATURES				
Application (minimum)	+ 10		°C	
Service (continuous)	- 40 to + 180		°C	
Short time	> 200		°C	

STORAGE and SHELF LIFE
Two years when stored at 21° C (70° F), 50 % relative humidity, out of direct sunlight.

Important – Information on the above characteristics is based upon tests we believe to be reliable. The values given are typical values that vary according to application conditions. The values are intended only as a source of information and are given without guarantee and do not constitute a warranty. Purchasers should independently determine prior to use the suitability of this material for their specific purposes.
All Avery Dennison materials described herein are sold subject to Avery Dennison's Conditions of Sales, a copy of which is available on request.

39.01

Avery Dennison – World Wide Specialty Tape Division

Europe – Belgium	☎ + 32 (14) 40 48 11	🖷 + 32 (14) 40 48 55
Asia Pacific – Singapore	☎ + 65 (273) 23 55	🖷 + 65 (278) 24 55
United States – Ohio	☎ + 1 (440) 358-2600	🖷 + 1 (440) 358 3298
Africa – South-Africa	☎ + 27 (11) 249 5700	🖷 + 27 (11) 472 2924
Website	www.averydennison.com	
E-mail	std@averydennison.com	

AVERY DENNISON

VITA

Byron Smith was born on the 20th day of May in 1983 to Daniel Smith and Teresa Bobbio in Suffolk, Virginia. He was raised in the greater Tidewater area and graduated from Deep Creek High School in August of 2000. While attending Deep Creek High Byron was active in a number of water related sports and played on the school's tennis team. Following his high school graduation, he matriculated to Virginia Commonwealth University, where he received a Bachelor of Science in Mechanical Engineering in 2005. While pursuing his undergraduate degree, he was awarded the EDC Scholarship for Art and Engineering for his work on piezoelectric phonograph needles.

Mr. Smith went on to pursue his graduate degree at Virginia Commonwealth University, where he received departmental support as a teaching assistant. While pursuing his Master's, he received the opportunity to conduct research at Konkuk University as a visiting scholar under the support of the National Science Foundation's East Asia and Pacific Summer Institute. Byron has co-authored works that have been published in *Smart Materials and Structures* and has presented findings at the conference for the SPIE's International Society for Optics Engineering, in 2007, as well as the ICEST Conference, held in Seoul South Korea in 2005.